Structural and Multidisciplinary Optimization (2022) 65:47
https://doi.org/10.1007/s00158-021-03137-1

RESEARCH PAPER

Acoustic topology optimization using moving morphable components in neural network-based design

Ki Hyun Kim[1] · **Gil Ho Yoon**[1]

Received: 30 July 2021 / Revised: 6 October 2021 / Accepted: 12 October 2021 / Published online: 18 January 2022

Abstract

In this study, we developed an acoustic topology optimization using moving morphable components (MMCs) for the design of two-dimensional sound reduction structures. MMC-based topology optimization has been developed for structural topology optimization; however, no extant study on the design of sound reduction structures has utilized MMC-based topology optimization. Instead of directly changing the distribution of pixel-wise materials to form the shape of a structure, MMC-based topology optimization changes the geometric and positional parameters of MMCs and forms the shape of a structure through the overlapping of MMCs. In this study, finite element analysis based on the Helmholtz equation was performed to calculate the acoustic performance of sound reduction structures. To complement the unsatisfactory performance of designs by local optimal points, we evaluated many designs optimized under different design conditions and optimization settings with respect to the original design condition. We also devised additional design procedures to improve the acoustic performance of sound reduction structures by exploring a lot of design samples modified from the designs based on MMC-based topology optimization. Owing to the rather long time required for repeated performance calculations, the performance was estimated by using a multilayer perceptron to roughly select the design samples that need to be evaluated by finite element analysis. Design examples for barrier structures and duct internal structures were considered to demonstrate the validity of the proposed approach.

Keywords Acoustic topology optimization · Moving morphable component · Artificial neural network · Multilayer perceptron · Sound reduction

1 Introduction

Topology optimization is a useful technique for designing the shape of structures. In the field of computational acoustics, topology optimization methods mainly employ gradient-based optimization algorithms (Kim and Yoon 2015, 2020; Yoon 2013; Yoon et al. 2018; Duhring et al. 2008; Christiansen et al. 2015; Kook et al. 2012, 2013; Goo et al. 2017; Lee and Kim 2009; Lee 2015). However, the solutions obtained by gradient-based optimization algorithms are not guaranteed to be near the global optimal points, but likely local optima; a design at a local optimal point for the intended design condition may not always be the best. This implies that a local optimal point for another design condition could provide a better design for the intended design condition. From this perspective, it is worth considering generating various optimized designs by changing the design conditions and optimization settings to determine an appropriate design for the intended design condition. In this case, further exploration of the design with better performance can be performed by generating partially modified designs from various pre-acquired designs. Computing the performances of a large number of partially modified designs can take a long time. Artificial neural networks (ANNs) can be used to select candidate designs that are expected to have relatively superior performance and, thus, reduce the computation time. Then, the most improved design for the intended design condition can be selected from among the candidate designs on the basis of the performance computation. In this context, the design of sound reduction structures using moving morphable component (MMC)-based topology

Responsible Editor: Xu Guo

✉ Gil Ho Yoon
ghy@hanyang.ac.kr; gilho.yoon@gmail.com

[1] School of Mechanical Engineering, Hanyang University, Seoul 04763, Republic of Korea

optimization and performance estimation by using a multilayer perceptron (MLP) was performed in this study.

1.1 Adoption of MMC-based topology optimization in acoustic problems

Topology optimization techniques based on the solid isotropic material with penalization (SIMP) method derive the shape of structures through the optimized distribution of pixel-wise materials. These are distinguished from size optimization techniques from the perspective that a basic shape is not provided. In acoustic problems, the presence of a pixel-wise material at a certain position can be represented by the material interpolation parameter that determines the material properties between air and a rigid material. For example, if the material interpolation parameter is equal to 1, a pixel-wise material is a rigid material. However, the material interpolation parameter of zero indicates that the pixel-wise material is air. In SIMP-based acoustic topology optimization, the material interpolation parameters of individual finite elements are appropriately defined for the implicit design variables assigned to each finite element. These implicit design variables are continuous between 0 and 1, similar to the material interpolation parameters. The SIMP method has been widely used in previous studies on the design of sound-related structures based on topology optimization. For example, sound barriers (Kim and Yoon 2015, 2020; Duhring et al. 2008; Kook et al. 2012), muffler partitions (Yoon 2013; Lee and Kim 2009; Lee 2015), acoustic focusers (Yoon et al. 2018), and structures inside a room or cavity (Duhring et al. 2008; Christiansen et al. 2015; Kook et al. 2013; Goo et al. 2017) were considered in SIMP-based acoustic topology optimization.

However, when utilizing acoustic topology optimization techniques, it is not easy to find appropriate local optimal solutions that can be regarded as a global optimal solution if there are many local optimal solutions with different shapes. The nature of the acoustic design problem affects the presence of various local optimal solutions. In this case, considering a plurality of local optimal solutions obtained under various optimization conditions may help to find out the global optimum design. For example, the initial values of design variables can be diversified for this purpose. In this context, obtaining various shapes through acoustic topology optimization is beneficial to discovering the design with the best performance. It may be considered desirable that the influence of the initial values of design variables on the optimization result is small, but it does not always guarantee the convergence to the global optimum point. Therefore, when local optima rather than global optimum are obtained, the sensitivity of local optima with respect to the initial design parameters may help to explore the solution space.

In our previous studies (Kim and Yoon 2015, 2020) on the SIMP-based topology optimization of sound reduction structures, it was difficult to obtain various shapes of structures because of the similar patterns of optimized material distributions according to the initial design variables. The initial values of the design variables did not significantly affect the optimized material distribution unless the finite element size was sufficiently small. In addition, the distribution of materials was restricted, owing to the use of filtering techniques that prevent intermediate materials, often called gray elements. An SIMP-based topological design is inherently difficult to modify through random variations in design variables. Therefore, SIMP-based topology optimization in acoustic problems may be disadvantageous for exploring the various shapes of structures with better acoustic performance.

In this study on the design of sound reduction structures, topology optimization based on MMCs is adopted as an alternative to SIMP-based topology optimization. Topology optimization based on MMCs, proposed by Guo et al. (2014), is a new technique in the field of structural topology optimization. Guo et al. (2014) proposed to represent the shape of a structure based on the layout of MMCs that can overlap each other. Zhang et al. (2016) improved the approach by Guo et al. (2014) by using the components of variable thicknesses. In contrast to many advances in MMC-based topology optimization in solid mechanics (Guo et al. 2016b; Deng and Chen 2016; Takalloozadeh and Yoon 2017; Zhang et al. 2018a; Lei et al. 2019; Lian et al. 2020), no extant study has considered acoustic topology optimization by using MMCs.

MMC-based topology optimization adopts explicit design variables related to geometric parameters such as the length, thickness, angle, and position of an MMC. To define the material interpolation parameters for the explicit design variables, a formulation based on a level-set function was considered. Compared with SIMP-based topology optimization, MMC-based topology optimization has the following advantages**.** The MMC-based topological design inherently has gray elements only at the boundary of the designed shape. In addition, different initial settings of design variables can provide different optimized shapes that are visually distinct. Because the design variables explicitly represent the geometric parameters, MMC-based topological designs can be partially modified through random variations in the design variables. Therefore, MMC-based topology optimization is effective for exploring various shapes of structures with better acoustic performance.

1.2 Design exploration procedures using performance estimation by multilayer perceptron

Additional design exploration procedures were developed for determining a new design exhibiting improved acoustic performance using designs obtained in advance by topology optimization. Figure 1 depicts the presented design procedures. First, basic design samples are prepared from the results of MMC-based topology optimization performed under different acoustic conditions and optimization settings. From the basic design samples, certain extracted design samples are selected based on the acoustic performances of the basic design samples under a given design condition. The mean sound pressure level (SPL) is used as an indicator of acoustic performance. The process of extracting the design samples and the subsequent processes are all performed under the same design conditions. Then, many modified design samples for additional design exploration are generated by subjecting the extracted design samples to random changes. Owing to the time cost of computing the acoustic performances of a large number of modified design samples, only the performances of certain modified design samples are computed. On the contrary, the performances of the other modified design samples are estimated by the MLP, which is modeled using the precomputed performances of certain modified design samples. Then, candidate design samples with relatively high estimated performances are selected from the remaining modified design samples that are not computed. Finally, the final design samples are selected by computing the accurate acoustic performances of the candidate design samples. The acoustic performances of the final design samples are expected to be better than those of the designs obtained solely by topology optimization.

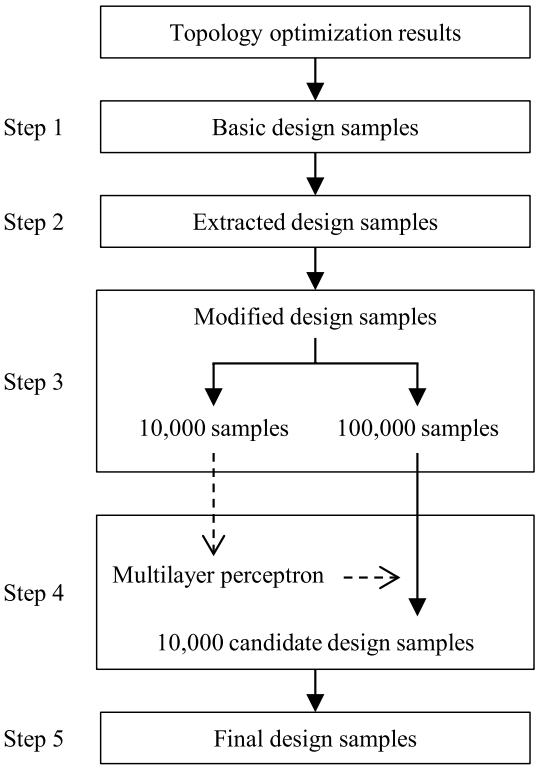

Fig. 1 Presented design procedures for finding the optimum designs

To build an artificial neural network that estimates the acoustic performance of MMC-based design data, an MLP was adopted in this study. Pixel-wise values representing the shape of the structure, that is, the material interpolation parameters, were used as inputs of the MLP. Although it is also possible to use the MMC-based design variables as inputs, this study adopted pixel-wise values considering the convenience of training an MLP. This study aimed to examine the possibility of using a simple MLP before using state-of-the-art ANN techniques in the design processes of acoustic structures. The application of advanced ANNs such as convolutional neural networks (CNNs) and various training techniques are considered for further research in the future.

Typical strategies utilizing ANNs in the computational design of structures can be broadly divided into two. One is to estimate the performances of the explored structures using ANNs, and the other is to estimate the optimized structures for the given design conditions. The strategy used in this study corresponds to the former. Regarding the former strategy, ANNs have been used as an approximate model for various physical performance indicators in computer-aided engineering. In the field of computational acoustics, to which this study belongs, MLPs have been used to predict the acoustic performance of design parameters (Durali and Delnavaz 2005; Yahya et al. 2010; Chang et al. 2018). Durali and Delnavaz (2005) modeled an MLP using the optimization parameters of a submarine shape as inputs and the acoustic pressure amplitude and phase at the reference point as outputs. Yahya et al. (2010) used an MLP to predict a classroom's reverberation time obtained by a finite element method (FEM). Chang et al. (2018) used an MLP in conjunction with muffler design parameters and sound transmission loss simulated by an FEM. In the field of computational fluid dynamics, ANNs have been used to mitigate high computational costs (Rai and Madavan 2001; Yilmaz and German 2017; Zhang et al. 2018b; Guo et al. 2016a). Rai and Madavan (2001) applied a two-layer ANN to predict the airfoil surface pressure for the aerodynamic design of a turbomachinery airfoil. Yilmaz and German (2017) predicted the airfoil pressure coefficient using CNNs that take the coordinates of the airfoil geometry as inputs. Zhang et al. (2018b) represented the airfoil geometry with an image-like array of pixels instead of a set of coordinates to apply a CNN to the prediction of lift coefficients. The pixels in the external space of the airfoil geometry

were colored with the freestream Mach number to combine the input information into a single data format. Guo et al. (2016a) proposed an approximation model based on a CNN for the real-time prediction of nonuniform steady laminar flow. In the field of computational solid mechanics, some studies have used ANNs to predict stress distributions (Liang et al. 2018; Nie et al. 2020). Liang et al. (2018) used a deep learning model to estimate the stress distribution of an aortic wall. Nie et al. (2020) predicted stress fields in cantilevered structures using CNNs.

Regarding the latter strategy, ANNs have been used as generative models to efficiently generate the optimal topological design of structures (Ulu et al. 2016; Sosnovik and Oseledets 2019; Yu et al. 2019; Li et al. 2019; Oh et al. 2019; Zheng et al. 2021a, 2021b). Ulu et al. (2016) proposed to project an optimal topology into a lower-dimensional space using principal component analysis (PCA) and constructed a fully connected ANN between the loading configurations and PCA weights for the optimal topology. Sosnovik and Oseledets (2019) used deep learning techniques to estimate the final result of optimization from the intermediate results of iterative topology optimization. Yu et al. (2019) predicted an optimized low-resolution structure according to the design conditions using a CNN-based encoder and decoder, and then generated an optimized high-resolution structure using a conditional generative adversarial network (GAN). Similarly, Li et al. (2019) used a GAN and super-resolution GAN to predict low-resolution and high-resolution structures for conductive heat transfer structures. Oh et al. (2019) proposed a design framework that integrated topology optimization and a GAN in an iterative manner to generate a large number of new designs. Zheng et al. (2021a, 2021b) predicted MMC-based (2021a) and SIMP-based (2021b) structural topologies based on the design conditions using U-Net neural networks.

The remainder of this paper is organized as follows. Section 2 describes the mathematical formulation for MMC-based acoustic topology optimization. Section 3 describes the design procedures for using an MLP to explore new designs with improved performance. Two design examples adopting the proposed approach are presented in Sect. 4. The conclusions of this work are drawn in Sect. 5.

2 MMC-based acoustic topology optimization

2.1 Acoustic finite element analysis

2.1.1 Finite element formulation of Helmholtz equation

In this study, the acoustic performance of two-dimensional structures was computed using the FEM applied to the Helmholtz equation in Eq. (1). In Eq. (1), ω, c, and p represent the angular frequency, speed of sound, and acoustic pressure, respectively. The weak formulation of the Helmholtz equation is expressed in Eq. (2). In Eq. (2), the virtual acoustic pressure $\tilde{p}$ is defined in the analysis domain Ω, and the component n_i of the outward unit normal vector is defined on the domain boundary Γ. To express the rigid domain as well as the wave propagation domain, the weak formulation is divided by the variable ρ, representing the material density. The three boundary conditions in Eq. (3) were used in the examples considered in this study, where p_{in} represents the amplitude of the acoustic pressure of an incident wave. Substituting Eq. (3) into Eq. (2) gives the equation for the numerical analysis in Eq. (4).

$$\left(\nabla^2 + \frac{\omega^2}{c^2}\right)p = 0 \tag{1}$$

$$\frac{\omega^2}{\rho c^2}\int \tilde{p}p \quad d\Omega - \frac{1}{\rho}\int \frac{\partial \tilde{p}}{\partial x_i}\frac{\partial p}{\partial x_i}d\Omega \quad + \frac{1}{\rho}\int \tilde{p}\frac{\partial p}{\partial x_i}n_i \quad d\Gamma = 0 \tag{2}$$

$$\frac{\partial p}{\partial x_i}n_i = \begin{cases} 0 \text{ for reflected waves} \\ -\mathrm{i}\dfrac{\omega}{c}p \text{ for outgoing waves} \\ -\mathrm{i}\dfrac{\omega}{c}p + 2\mathrm{i}\dfrac{\omega}{c}p_{in} \text{ for outgoing waves and incedent waves} \end{cases} \tag{3}$$

$$\frac{\omega^2}{\rho c^2}\int \tilde{p}p d\Omega - \frac{1}{\rho}\int \frac{\partial \tilde{p}}{\partial x_i}\frac{\partial p}{\partial x_i}d\Omega - \mathrm{i}\frac{\omega}{\rho c} \int \tilde{p}p d\Gamma_{out} = -2\mathrm{i}\frac{\omega}{\rho c}p_{in}\int \tilde{p}d\Gamma_{in}, \tag{4}$$

A discretized form of Eq. (4) for a single finite element is shown in Eq. (5), where the unknown vector $\{p\}$ represents the values of the acoustic pressure at the four nodes of a square finite element. The local matrices $[M]$, $[K]$, $[M_{bc}]$, and $[f_{bc}]$ are formed by the linear shape function $[N]$ and the differentiated shape function $[B_i]$, as shown in Eq. (6). The bulk modulus B and characteristic impedance z are defined in Eqs. (7). The matrix equation for the entire analysis domain is expressed in Eq. (8), where the unknown vector $\mathbf{p}$ represents the values of the acoustic pressure at all nodes in the discretized analysis domain. The global matrices $\mathbf{M}$, $\mathbf{K}$, $\mathbf{M}_{bc}$, and $\mathbf{f}_{bc}$ are constructed by assembling local matrices, as shown in Eq. (9). Subsequently, the matrix equation $\mathbf{Ap} = \mathbf{b}$ is solved.

$$\left[\frac{\omega^2}{B}[M] - \frac{1}{\rho}[K] - \mathrm{i}\frac{\omega}{z}[M_{bc}]\right]\{p\} = -2\mathrm{i}\frac{\omega}{z}p_{in}[f_{bc}], \tag{5}$$

$$[M] = \int [N]^{\mathrm{T}}[N]d\Omega,\ [K] = \int [B_i]^{\mathrm{T}}[B_i]d\Omega,\ [M_{bc}] = \int [N]^{\mathrm{T}}[N]d\Gamma_{out}, \{f_{bc}\} = \int [N]^{\mathrm{T}}d\Gamma_{in}, \tag{6}$$

$$B = \rho c^2, \quad z = \rho c, \tag{7}$$

$$\left[\omega^2\mathbf{M} - \mathbf{K} - \mathrm{i}\omega\mathbf{M}_{bc}\right]\mathbf{p} = -2\mathrm{i}\omega p_{in}\mathbf{f}_{bc} \rightarrow \mathbf{Ap} = \mathbf{b}, \tag{8}$$

$$\mathbf{M} = \left\langle \frac{1}{B}[M] \right\rangle, \quad \mathbf{K} = \left\langle \frac{1}{\rho}[K] \right\rangle, \quad \mathbf{M}_{bc} = \left\langle \frac{1}{z}[M_{bc}] \right\rangle, \quad \mathbf{f}_{bc} = \left\langle \frac{1}{z}\{f_{bc}\} \right\rangle \langle\rangle : \text{ assemble for all elements.} \tag{9}$$

2.1.2 Material representation by interpolation parameters

The material states of the finite elements in the design area are determined by the material interpolation parameter γ_j assigned to each finite element, as shown in Fig. 2. The material interpolation parameter γ_j has a value between 0 and 1, where a value of 0 represents air, 1 represents a rigid material, and any intermediate vale represents an intermediate material. The vector $\boldsymbol{\gamma}$ is defined for the n material interpolation parameters in Eq. (10). As Eq. (11), the inverse density ρ_{inv} and the inverse bulk modulus B_{inv} of the j-th finite element are interpolated linearly for the material interpolation parameter γ_j between the two material states of air and a rigid material. The subscripts "a" and "r" represent air and a rigid material, respectively. The material properties used for air and a rigid material are listed in Table 1. It should be noted that the intermediate materials that appear in the topology optimization results are replaced by air or a rigid material by discretization of the material interpolation parameters.

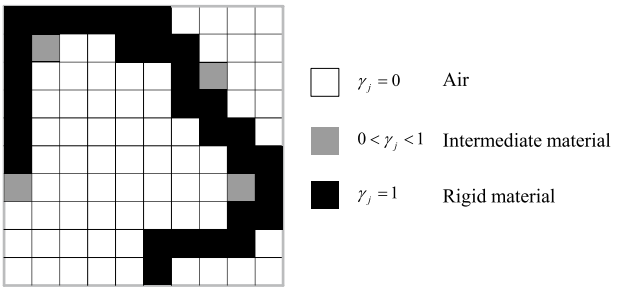

Fig. 2 Shape of the structure represented by the distribution of materials in design area

$$\boldsymbol{\gamma} = [\gamma_1, \ldots, \gamma_j, \ldots, \gamma_n]^{\mathrm{T}} \quad (0 \le \gamma_j \le 1), \tag{10}$$

$$\rho_{inv} = \frac{1}{\rho} = \frac{1}{\rho_a} + \left(\frac{1}{\rho_r} - \frac{1}{\rho_a}\right) \times \gamma_j, \quad B_{inv} = \frac{1}{B} = \frac{1}{B_a} + \left(\frac{1}{B_r} - \frac{1}{B_a}\right) \times \gamma_j. \tag{11}$$

2.1.3 Acoustic performance indicators

In this study, two acoustic indicators were considered in relation to the objective function of optimization problems. One is the squared amplitude of the acoustic pressure, and the other is the SPL. These indicators are expressed by the acoustic pressure p_i at the i-th finite element node, as shown in Eq. (12) and Eq. (13), respectively. The acoustic pressure p_i is expressed by the acoustic pressure vector $\mathbf{p}$, as shown in Eq. (14) using the row vector $\mathbf{L}_i$, which has one element equal to 1 and the other elements equal to 0. Using the derivatives of the acoustic pressure p_i in Eq. (14), the derivatives of the two indicators for the interpolation parameters are formulated as in Eq. (15) and Eq. (16), respectively. The symbols Re and conj represent the real part and complex conjugate of a complex number, respectively. The common logarithm and natural logarithm are represented by log and ln, respectively.

$$\text{Squared amplitude of acoustic pressure} : \left|p_i\right|^2, \tag{12}$$

$$\text{Sound pressure level} : SPL_i = 10\log\frac{\left|p_i\right|^2}{\left|p_{ref}\right|^2} \quad \left(p_{ref} = 2 \times 10^{-5}\ \text{Pa}\right) \tag{13}$$

$$p_i = \mathbf{L}_i\mathbf{p} \rightarrow \frac{\partial p_i}{\partial \gamma_j} = \mathbf{L}_i\left(-\mathbf{A}^{-1}\frac{\partial \mathrm{A}}{\partial \gamma_j}\mathbf{p}\right), \tag{14}$$

$$\frac{\partial f_{SA}}{\partial \gamma_j} = 2\ \mathrm{Re}\left[\mathrm{conj}(p_i)\frac{\partial p_i}{\partial \gamma_j}\right] = 2\ \mathrm{Re}\left[-\mathrm{conj}(p_i)\mathbf{L}_i\mathbf{A}^{-1}\frac{\partial \mathrm{A}}{\partial \gamma_j}\mathbf{p}\right], \tag{15}$$

Table 1 Material properties used for air and a rigid material

Material type	Density	Speed of sound	Bulk modulus	Characteristic impedance
Air	$\rho_a = 1.25\ \mathrm{kg\ m^{-3}}$	$c_a = 343\ \mathrm{m\ s^{-1}}$	$B_a = \rho_a c_a^2$	$z_a = \rho_a c_a$
Rigid material	$\rho_r = \rho_a \times 10^7$	$c_r = c_a \times 10$	$B_r = \rho_r c_r^2$	$z_r = \rho_r c_r$

$$\frac{\partial f_{SPL}}{\partial \gamma_j} = 2 \quad \mathrm{Re}\left[10\frac{1}{p_i \ln 10}\frac{\partial p_i}{\partial \gamma_j}\right] = 2 \quad \mathrm{Re}\left[-10\frac{1}{p_i \ln 10}\mathbf{L}_i\mathbf{A}^{-1}\frac{\partial \mathrm{A}}{\partial \gamma_j}\mathbf{p}\right]. \tag{16}$$

2.2 Design parameterization using moving morphable components

This subsection describes the manner in which the material interpolation parameters are parameterized using MMC-based design variables. First, the expression of the material interpolation parameters for the geometric parameters of MMCs is described. Then, the expression of the geometric parameters for the design variables is described.

2.2.1 Parameterization of material interpolation parameters for geometric parameters

The parameterization of material interpolation parameters for the geometric parameters of MMCs essentially follows the method presented in the literature on structural topology optimization based on MMCs (Guo et al. 2014; Zhang et al. 2016). Figure 3 depicts the calculation process of the material interpolation parameter from geometric parameters of MMCs. As Eq. (17), the material interpolation parameter γ of each finite element is determined by the value of the function $\phi_s(x, y)$ at the center point of the corresponding finite element. The coordinate $(x_{center,j}, y_{center,j})$ of the center point is defined for the origin point located at the lower-left point of the design area. The function $\phi_s(x, y)$ represents the shape of a structure that is determined by the geometric parameters of the MMCs. The function $\phi_s(x, y)$ is formulated using the level-set function ϕ_k, the approximate Heaviside function $\phi_{h,k}$, and the Max function, as shown in Eq. (18).

$$\gamma_j = \phi_s(x = x_{center,j}\,,\ y = y_{center,j}), \tag{17}$$

$$\begin{aligned}\phi_k(L_k,\ t_k,\ \theta_k,\ x_{0,k},\ y_{0,k},\ x,\ y) \ \rightarrow\ \phi_{h,k}(\phi_k) \ \rightarrow\ \phi_s \\ = \mathrm{Max}(\phi_{h,k=1},\ \phi_{h,k=2},\ \phi_{h,k=3},\ \ldots).\end{aligned} \tag{18}$$

The level-set function ϕ_k for a single MMC is expressed by Eq. (19), where parameters A_k and B_k are defined in Eq. (20). The geometric parameters L_k, t_k, θ_k, $x_{0,k}$, and $y_{0,k}$ represent the length, thickness, angle, and x- and y-coordinates of the k-th MMC, respectively. The exponential n is an even integer, and $n = 6$ was used in this study. The area where the level-set function satisfies $\phi_k > 0$ represents the shape of a single component. To limit the values of the level-set function between zero and one, the approximate Heaviside function is applied to the level-set function, as shown in Eq. (21). To represent the overlap of multiple components,

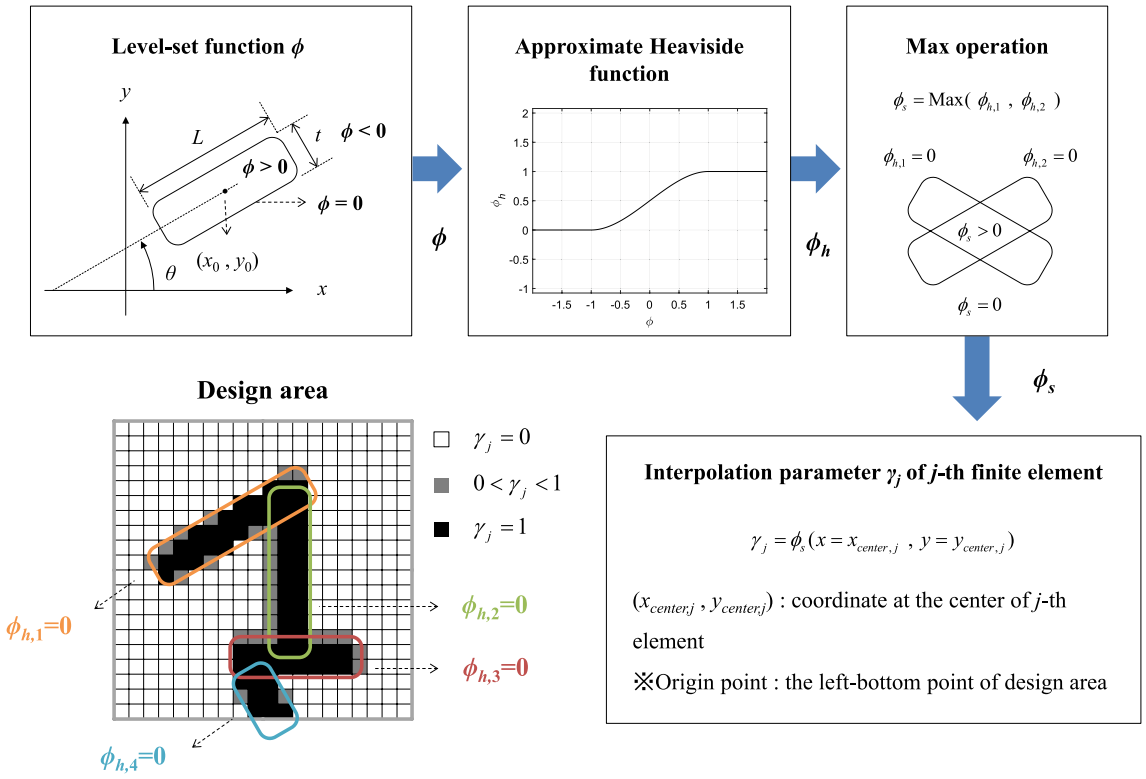

Fig. 3 Calculation process of material interpolation parameter from geometric parameters of MMCs

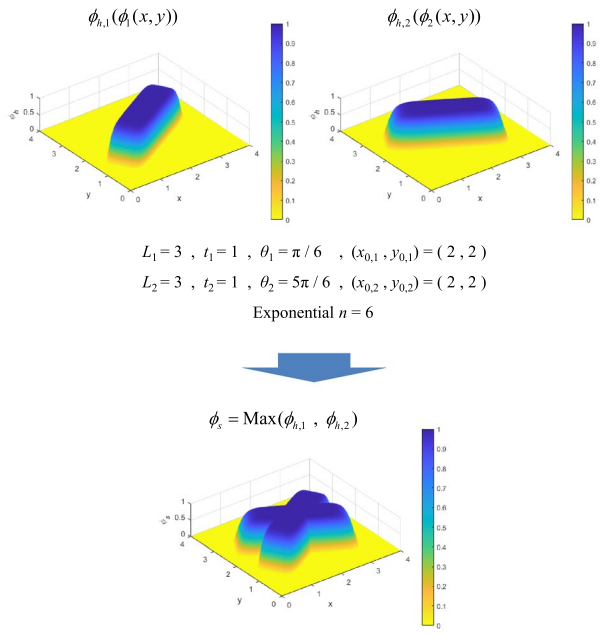

Fig. 4 Visualized approximate Heaviside function applied to the level-set function

the Max function is applied to the multiple approximate Heaviside functions, as shown in Eq. (22), where n_c is the number of MMCs. The upper part of Fig. 4 depicts a visualization example of the approximate Heaviside function applied to the level-set function. It is shown that the approximate Heaviside function decreases sharply from 1 to 0 near the edges of the component. The lower part of Fig. 4 shows a visualization example of function ϕ_s, which represents the shape formed by two components.

$$\phi_k = -\left(\frac{2A_k}{L_k}\right)^n - \left(\frac{2B_k}{t_k}\right)^n + 1, \tag{19}$$

$$\begin{aligned} A_k &= \cos\theta_k \cdot (x - x_{0,k}) + \sin\theta_k \cdot (y - y_{0,k}), B_k \\ &= -\sin\theta_k \cdot (x - x_{0,k}) + \cos\theta_k \cdot (y - y_{0,k}), \end{aligned} \tag{20}$$

$$\phi_{h,k} = \begin{cases} 0 & \text{if } \phi_k \le 1 \\ \frac{3}{4}\left(\phi_k - \frac{\phi_k^3}{3}\right) + \frac{1}{2} & \text{if } -1 \le \phi_k \le 1 \\ 1 & \text{if } \phi_k > 1 \end{cases} \tag{21}$$

$$\phi_s = \mathrm{Max}(\,\phi_{h,k}\,) \quad k = 1, \ldots, n_c. \tag{22}$$

The derivative of the function ϕ_s for each of the geometric parameters was calculated using the chain rule in Eq. (23) without using the finite-difference method. Both the level-set function and approximate Heaviside function are continuously differentiable. Although the Max function is nondifferentiable, its derivative can be defined by Eq. (24).

$$\frac{\partial \phi_s}{\partial(L_k,\, t_k,\, \theta_k,\, x_{0,k},\, y_{0,k})} = \frac{\partial \phi_s}{\partial \phi_{h,k}} \frac{\partial \phi_{h,k}}{\partial \phi_k} \frac{\partial \phi_k}{\partial(L_k,\, t_k,\, \theta_k,\, x_{0,k},\, y_{0,k})}, \tag{23}$$

$$\frac{\partial \phi_s}{\partial \phi_{h,k}} = \begin{cases} 1 & \text{if } \phi_{h,k} = \phi_s \\ 0 & \text{if } \phi_{h,k} \ne \phi_s \end{cases} \tag{24}$$

2.2.2 Parameterization of geometric parameters for design variables

This study adopted continuous design variables between zero and one, as shown in Eq. (25) instead of directly using the geometric parameters of MMCs as design variables. In this case, each design variable interpolates the minimum and maximum values of each geometric parameter, as shown in Eq. (26), where D_{design} and H_{design} represent the lengths of the design area in the x and y directions, respectively. Under this treatment, the geometric parameters of different ranges can be updated to an appropriate extent using the optimization algorithm. When the thicknesses of the MMCs are fixed to a constant middle value, that is, $t_k = (t_{\min} + t_{\max})/2$, the number of design variables is reduced to $4n_c$. In this case, the order of the design variables assigned to the other geometric parameters is the same as the order in Eq. (26).

$$\mathbf{x} = [x_1, \ldots, x_i, \ldots, x_{5\times n_c}]^{\mathrm{T}}, \quad 0 \le x_i \le 1, \tag{25}$$

$$\begin{Bmatrix} L_k \\ t_k \\ \theta_k \\ x_{0,k} \\ y_{0,k} \end{Bmatrix} = \begin{Bmatrix} L_{\min} + (L_{\max} - L_{\min}) \times x_k \\ t_{\min} + (t_{\max} - t_{\min}) \times x_{n_c+k} \\ \theta_{\max} \times x_{2\times n_c+k} \\ D_{design} \times x_{3\times n_c+k} \\ H_{design} \times x_{4\times n_c+k} \end{Bmatrix} (1 \le k \le n_c) \tag{26}$$

2.3 Formulation of optimization problem

2.3.1 Setup of optimization problem

The formulation of the optimization problem used for the design examples considered in this study is expressed as shown in Eq. (27). The objective function $f(\mathbf{x})$ and the constraint function $g(\mathbf{x})$ are adjusted by the artificial variables y and z to prevent the optimal point from becoming infeasible. The objective function f is defined as the mean value of the acoustic performance in the measurement area, as shown in

Eq. (28). The acoustic performance can be either the squared amplitude of the acoustic pressure ($|p|^2$) or the SPL. The gradient of the objective function for the design variable vector $\mathbf{x}$ can be expressed using the chain rule in Eq. (29), where n is the number of material interpolation parameters γ, that is, the number of finite elements in the design area. The constraint g is formulated as in Eq. (30), where the constraint parameter b represents the maximum occupancy rate of the rigid materials in the design area. In this study, the constraint parameter b can be set to its maximum value ($b=1$), owing to the inherent size limits of the MMCs.

$$\begin{aligned} &\text{Minimize } f(\mathbf{x}) + z + 10^5 y \\ &\mathbf{x} = [x_1\,,\,\ldots\,,\,x_i\,,\,\ldots\,,\,x_{n_d}]^{\mathrm{T}} \\ &\text{subject to } g(\mathbf{x}) - y \le 0 \quad , \\ &0 \le x_i \le 1 \\ &y \ge 0,\ z \ge 0 \end{aligned} \tag{27}$$

$$f = \mathrm{Mean}\left(|p_i|^2\right) \text{ or } f = \mathrm{Mean}\left(SPL_i\right), \tag{28}$$

$$\frac{\partial f}{\partial \mathbf{x}} = \sum_{j=1}^{n} \frac{\partial f}{\partial \gamma_j}\frac{\partial \gamma_j}{\partial \mathbf{x}} = \left(\frac{\partial f}{\partial \boldsymbol{\gamma}^{\mathrm{T}}}\frac{\partial \boldsymbol{\gamma}}{\partial \mathbf{x}^{\mathrm{T}}}\right)^{\mathrm{T}}, \tag{29}$$

$$g = \frac{1}{n}\sum_{j=1}^{n}\gamma_j - b\,,\ \frac{\partial g}{\partial \mathbf{x}} = \frac{1}{n}\sum_{j=1}^{n}\frac{\partial \gamma_j}{\partial \mathbf{x}}. \tag{30}$$

In this study, the method of moving asymptotes (MMA), which is widely used in the field of topology optimization, was used as a gradient-based optimization algorithm. The MMA algorithm solves a subproblem approximated by moving asymptotes in each iteration step to update the design variables toward the optimal point. The solution of the subproblem in the current iteration step becomes the initial value of the subproblem in the next iteration step.

The lower asymptote L and the upper asymptote U of each design variable in the current iteration step (k) are calculated using the lower and upper asymptotes in the previous iteration step ($k-1$), as shown in Eq. (31). In the first two iteration steps ($k \le 2$), however, the lower asymptote L and the upper asymptote U are determined by the lower constraint $\underline{x}$ and the upper constraint $\overline{x}$ of design variables using the parameter s_{init}. The values of the lower and upper constraints $\underline{x}$ and $\overline{x}$ are 0 and 1, respectively, as defined in Eq. (27). After the first two iteration steps ($k > 2$), the parameter s determined by the convergence tendency of design variables in the previous two iteration steps adjusts the moving asymptotes, as shown in Eq. (32). If the parameter s is greater than 1, the asymptotes move farther away from the design variable than in the previous iteration step. In the opposite case, the asymptotes move closer to the design variable. In this study, the value of the parameter s_{init} is set to 0.5 and the value of the parameter s is set to 1.2/0.7, referring to the studies by Svanberg (1998, 2007). As suggested by Svanberg (1987), the lower move limit α and upper move limit β are also defined as in Eq. (33) to prevent the possibility of "division by zero".

$$\begin{aligned} &\text{if } k \le 2\text{:}\quad L_i^{(k)} = x_i^{(k)} - s_{init}(\overline{x} - \underline{x}),\quad U_i^{(k)} = x_i^{(k)} + s_{init}(\overline{x} - \underline{x}) \\ &\text{if } k > 2\text{:}\quad L_i^{(k)} = x_i^{(k)} - s(x_i^{(k-1)} - L_i^{(k-1)}),\quad U_i^{(k)} = x_i^{(k)} + s(U_i^{(k-1)} - x_i^{(k-1)}), \end{aligned} \tag{31}$$

$$\begin{cases} s = 1.2 & \text{if } (x_i^{(k)} - x_i^{(k-1)})(x_i^{(k-1)} - x_i^{(k-2)}) > 0 \\ s = 0.7 & \text{if } (x_i^{(k)} - x_i^{(k-1)})(x_i^{(k-1)} - x_i^{(k-2)}) < 0 \end{cases}, \tag{32}$$

$$\begin{aligned} \alpha_i^{(k)} &= 0.9L_i^{(k)} + 0.1x_i^{(k)} \\ \beta_i^{(k)} &= 0.9U_i^{(k)} + 0.1x_i^{(k)}. \end{aligned} \tag{33}$$

Based on the original MMA algorithm, the move range δ, which represents the maximum change in the design variables, was additionally defined in this study to find the local optimal point more effectively. Therefore, the possible range for updating the design variables at each iteration step is expressed as Eq. (34). If the objective function value does not decrease at the next iteration step, the design variables are updated again with the reduced value of the move range. The move range is gradually reduced by multiplying the current move range by 0.8 until the objective function value of the next iteration step is decreased. The initial value of the move range is set to 0.01, considering the appropriate search of a local optimal point and the affordable time cost in repeated computational experiments. The iterative process of optimization ends when the stop criteria in Eq. (35) are met.

$$\max(0\,,\,x_i^{(k)} - \delta^{(k)}\,,\,\alpha_i^{(k)}) < x_i^{(k)} < \min(1\,,\,x_i^{(k)} + \delta^{(k)}\,,\,\beta_i^{(k)}), \tag{34}$$

$$\delta < 10^{-3} \quad \text{or } k = 500. \tag{35}$$

2.3.2 Postprocessing of acoustic topology optimization results

From the optimization results, the values of the material interpolation parameters are discretized to 0 or 1 by comparison with 0.9, as shown in Eq. (36), to represent a structure consisting of only rigid materials. Here, some readers may have a question why the criterion value for discretization is set to 0.9. One may simply uses 0.5 as this value. But, as shown in Table 2, the material properties calculated according to Eq. (11) by the material interpolation parameters under 0.9 do not represent a solid material that interrupts the transmission of sound. A simple numerical example is provided to

validate this argument, as shown in Fig. 5. When a straight duct with incident waves is considered, an area of adjusted material properties is imposed at the middle of the duct to test the effect of intermediate materials on the mean SPL at the outlet area. The area of adjusted material properties has four square finite elements in horizontal direction. Table 3 shows the calculation results for the mean SPL according to the values of the material interpolation parameters that determine the intermediate material properties. Compared with the mean SPL when no intermediate material exists, that is, "$\gamma_j = 0$" representing air, the result from "$\gamma_j = 0.5$" indicates very slightly lowered mean SPL. Considering the entire results in Table 3, 0.9 was chosen as the criterion value for discretization. In terms of the acoustic performance after postprocessing, the best criterion value is different for each optimization result. As it is not possible to determine the best criterion value that can be applied in common, 0.9 can be used as an appropriate criterion value. In addition, since the sum of the material interpolation parameters decreases in most cases when postprocessing is performed based on 0.9, the constraint on material usage is still valid after postprocessing. Of course, since the shape by MMCs has its own maximum size, consideration for this is actually unnecessary.

$$\begin{aligned} &\gamma \to 0 \text{ if } \gamma \le 0.9, \\ &\gamma \to 1 \text{ if } \gamma > 0.9 \end{aligned} \tag{36}$$

3 Additional design procedures using multilayer perceptron

3.1 Description of presented design procedures

In this subsection, additional design procedures are presented to improve the acoustic performance of the sound reduction structure designed by MMC-based topology optimization. The detailed design procedures from the topology optimization results to the final designs are described step by step in Fig. 6.

3.1.1 Generation of basic design samples

In step 1, the basic design samples are prepared from various topology optimization results that are obtained by changing some design conditions such as the sound source position, sound measurement area, and frequency of the sound source. In addition, optimization settings, such as the objective function and the initial values of the design variables, can be changed to obtain various optimization results. The obtained structure after postprocessing is considered as the basic design sample.

Table 2 Material properties calculated according to Eq. (11) by the material interpolation parameters

γ_j	0	0.5	0.8	0.9	0.95	0.99	0.999	1
ρ (kg m^{-3})	1.25	2.50	6.25	1.25×10^{1}	2.50×10^{1}	1.25×10^{2}	1.25×10^{3}	1.25×10^{7}
B (kg m^{-3} s^{-2})	1.47×10^{5}	2.94×10^{5}	7.35×10^{5}	1.47×10^{6}	2.94×10^{6}	1.47×10^{7}	1.47×10^{8}	1.47×10^{14}

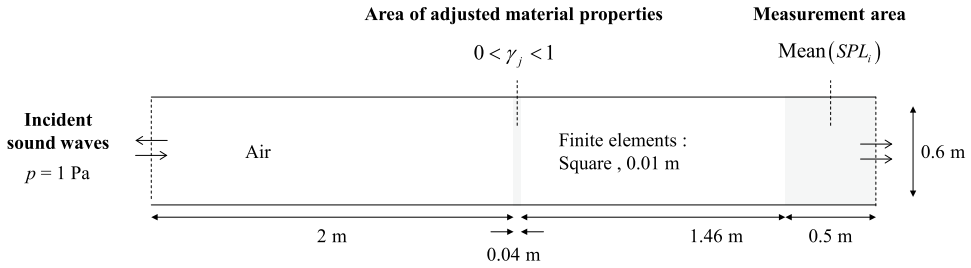

Fig. 5 Simple numerical example to test the effect of intermediate materials

Table 3 Mean SPL according to the values of the material interpolation parameters that determine the intermediate material properties for the test example in Fig. 5

γ_j	0	0.5	0.8	0.9	0.95	0.99	0.999	1
Mean SPL at 100 Hz (dB)	93.98	93.97	93.85	93.44	92.12	82.40	62.71	− 17.30
Mean SPL at 200 Hz (dB)	93.98	93.93	93.48	92.15	89.04	76.63	56.71	− 23.32
Mean SPL at 300 Hz (dB)	93.98	93.87	92.93	90.63	86.40	73.20	53.23	− 26.84

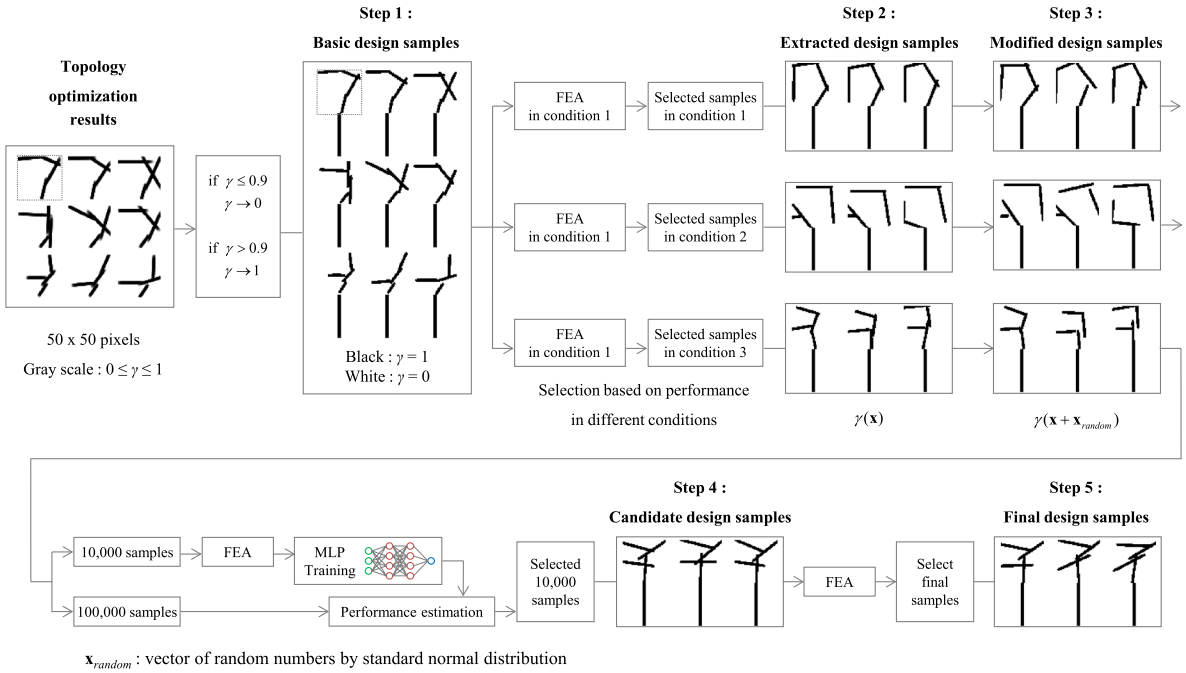

Fig. 6 Detailed design procedures from topology optimization results to final designs

3.1.2 Selection of extracted design samples

In step 2, relatively superior design samples are extracted from the basic design samples based on the acoustic performance calculated using finite element analysis (FEA) for a specific design condition. These extracted design samples are used in the remainder of the design procedures. The extraction of design samples is necessary for the effective exploration of design samples that will be additionally generated by partial modification. This is related to the training of the MLP considered in step 4. The high diversity and complexity of the training data used in the modeling of an ANN make it difficult to train the ANN. The number of extracted design samples can be appropriately selected according to design problems.

3.1.3 Generation of modified design samples

In step 3, the modified design samples are generated from the extracted design samples by adding a random number N_{random} to the design variable, as shown in Eq. (37). The random number is drawn from a normal distribution with a mean value of 0 and a standard deviation of 0.02, which results in a slight shape change in the modified design sample. Owing to the nature of the normal distribution, the number of design samples with relatively small modifications is greater than the number of design samples with relatively large modifications. In the modification of the design sample, MMCs connected to each other can be separated. Conversely, separated MMCs can be connected to each other. For each of the extracted design samples, multiple modified design samples are generated by applying different sets of random numbers. In this way, 110,000 modified design samples are generated from the extracted design samples.

$$x_i + N_{random} \rightarrow x_i. \tag{37}$$

3.1.4 Selection of candidate design samples

In step 4, candidate design samples are selected from the modified design samples using an MLP. Of the 110,000 modified design samples, 10,000 samples are used as training data for the MLP. Therefore, the acoustic performances of these 10,000 samples are calculated using FEA. The input and output of the MLP represent the design information and the estimated value of the acoustic performance, respectively. Using the constructed MLP, the performances of the remaining 100,000 samples are estimated. From the 100,000 design samples, the top 10,000 design samples are selected as candidate design samples based on the estimated performance.

3.1.5 Selection of final design samples

In step 5, the accurate acoustic performances of 10,000 candidate design samples are calculated using FEA. Then, the design samples ranked at the top in terms of the accurate performance are selected as the final design samples. The final design samples are also compared with several top design samples out of the 10,000 modified design samples used to train the MLP.

3.2 Modeling of multilayer perceptron

In this study, an MLP that estimates the acoustic performance of a structure under a specific acoustic condition was constructed using a dataset obtained from the MMC-based topology optimization and acoustic FEA.

3.2.1 Calculation process in multilayer perceptron

Figure 7 represents an MLP that computes the output vector from the input vector through a series of operations. In this study, the input vector $\mathbf{x}$ represents a set of material interpolation parameters for topological design, as shown in Eq. (38). The symbol $\mathbf{x}$ in Eq. (38) is used differently from the symbol $\mathbf{x}$ in Eq. (27), which represents a design variable vector for topology optimization. As shown in Fig. 7, an MLP has multiple hidden layers and one output layer. Each hidden layer performs a linear operation and then a nonlinear operation, as shown in Eq. (39), where the nonlinear operation $R(x)$ represents the rectified linear unit (ReLU) function. The output layer performs only a linear operation without a nonlinear operation, as shown in Eq. (40). In this study, the output vector from the output layer has only one component, that is, the output value f_{est}. The output value f_{est} is

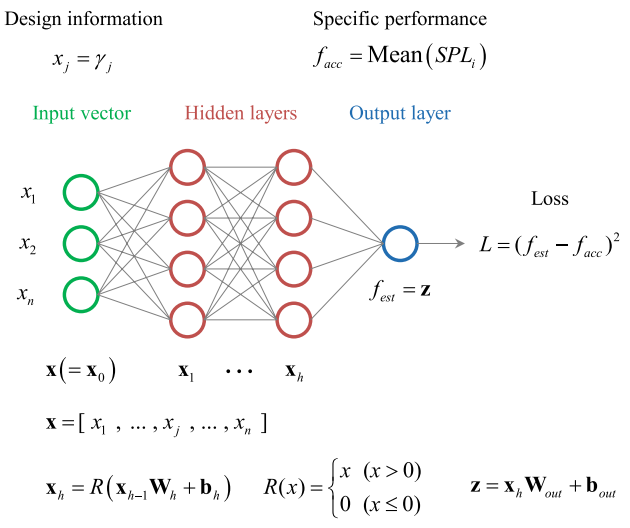

Fig. 7 Diagram of MLP

the estimated value of the accurate value f_{acc} corresponding to the input vector. The accurate value f_{acc} is set to the mean value of the SPL in the measurement area for a topological design given as input, as expressed in Eq. (41).

$$\mathbf{x} = [x_1, \ldots, x_j, \ldots, x_n], \quad x_j = \gamma_j, \tag{38}$$

$$\mathbf{x}_h = R(\mathbf{x}_{h-1}\mathbf{W}_h + \mathbf{b}_h), \quad R(x) = \begin{cases} x(x > 0) \\ 0(x \le 0) \end{cases} \tag{39}$$

$$f_{est} = \mathbf{z} = \mathbf{x}_h\mathbf{W}_{out} + \mathbf{b}_{out}, \tag{40}$$

$$f_{acc} = \mathrm{Mean}(SPL_i). \tag{41}$$

3.2.2 Training of multilayer perceptron

In the training process of the MLP, the weight matrices $\mathbf{W}$ and bias vectors $\mathbf{b}$ of the layers are optimized to generate the estimated value closest to the accurate value f_{acc}. The loss value L in Eq. (42) represents the square of the error between the estimated value f_{est} and the accurate value f_{acc}. To consider the mean of the loss values for a batch of input vectors, the batch loss value L_{batch} is defined by Eq. (43), where the batch size N_{batch} represents the number of input vectors in the batch. This batch loss value L_{batch} is used as an objective function of the optimization problem for the weight matrices $\mathbf{W}$ and bias vectors $\mathbf{b}$. In this study, the weight matrices and bias vectors were updated using the gradient descent method, as shown in Eq. (44), where η denotes the learning rate. One completion of sequential updates for all batches of input vectors is called an epoch. For multiple epochs, the composition of the batches changes in each epoch. The initial values of the weight matrices are set to random numbers drawn from a normal distribution, and the initial values of the bias vectors are set to zero.

$$L = (f_{est} - f_{acc})^2, \tag{42}$$

$$L_{\mathrm{batch}} = \frac{\overbrace{L_{\mathrm{sample1}} + L_{\mathrm{sample2}} + \cdots}^{N_{\mathrm{batch}}}}{N_{\mathrm{batch}}}, \tag{43}$$

$$\mathbf{W}_{\mathrm{updated}} = \mathbf{W} - \eta\frac{\partial L_{\mathrm{batch}}}{\partial \mathbf{W}}, \quad \mathbf{b}_{\mathrm{updated}} = \mathbf{b} - \eta\frac{\partial L_{batch}}{\partial \mathbf{b}}. \tag{44}$$

In this study, approximately 64%, 16%, and 20% of the total dataset were used as the training, validation, and test datasets, respectively. The validation dataset was used to determine whether the MLP was appropriately trained and

to adjust the hyperparameters for training. The basic hyperparameters are the batch size N_{batch}, number of hidden layers, size of each hidden layer (called the number of nodes), mean and standard deviation of initial weights, learning rate η, and number of epochs.

4 Design examples

In this section, three design examples for barrier structures, duct internal structures, and ground structures are presented using the proposed MMC-based topology optimization and additional design procedures. The objectives of the presented design examples are to investigate the shape of a two-dimensional structure in the design area that minimizes the mean SPL in the measurement area under a specific design condition. The size of the design area is 0.5 m × 0.5 m. The entire acoustic domain for FEA is discretized by 4-node square elements of side length 0.01 m.

The structure to be investigated can be understood as the cross-sectional shape of a regular three-dimensional structure in two-dimensional sound wave assumption as depicted in Fig. 8. In the case of designing a regular 3D structure, it is possible to expand the MMC-based acoustic topology optimization presented in this study to 3D acoustic topology optimization. However, in the case of designing an irregular 3D structure, it is necessary to define a mathematical model representing the material interpolation parameters in 3D space for the geometric parameters of 3D MMCs.

4.1 Setup of three design problems

The design example for barrier structures is configured as shown in Fig. 9. In this example, the upper part of a vertical

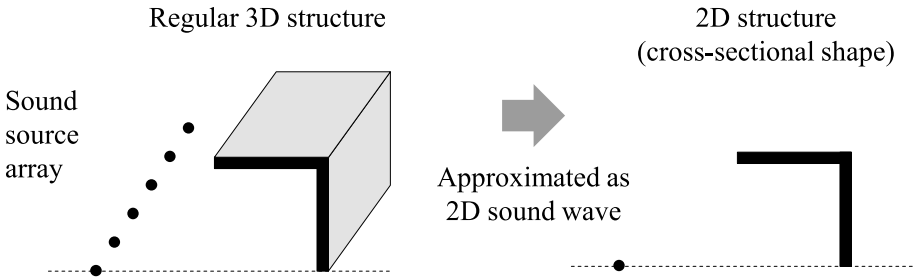

Fig. 8 Diagram for 2D structure as the cross-sectional shape of a regular 3D structure in 2D sound wave assumption

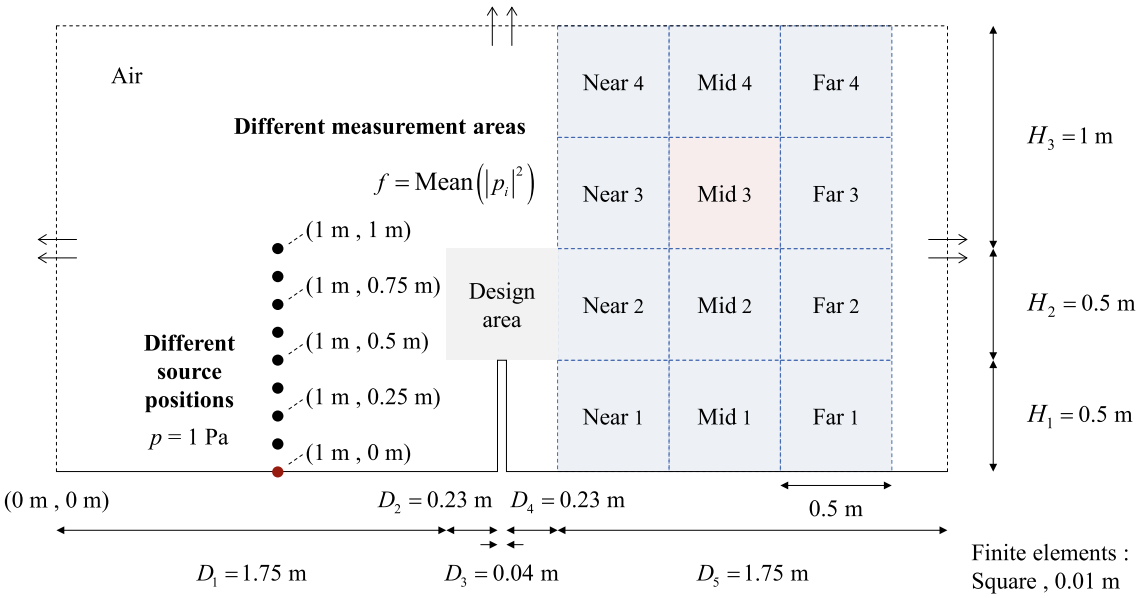

Different frequencies : f_s = 100 Hz, 110 Hz , … , 290 Hz, 300 Hz

※ 9 source positions x 12 measurement area x 21 frequencies → 2268 results

Fig. 9 Acoustic analysis conditions for the acoustic barrier including design area

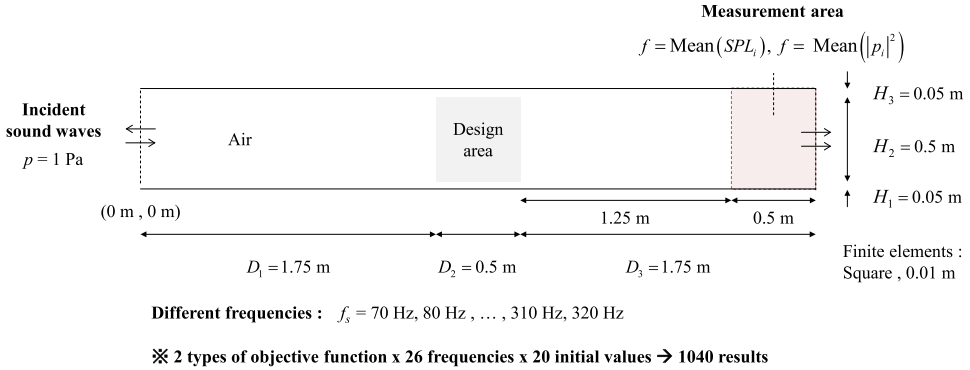

Fig. 10 Acoustic analysis conditions for the duct including internal design area

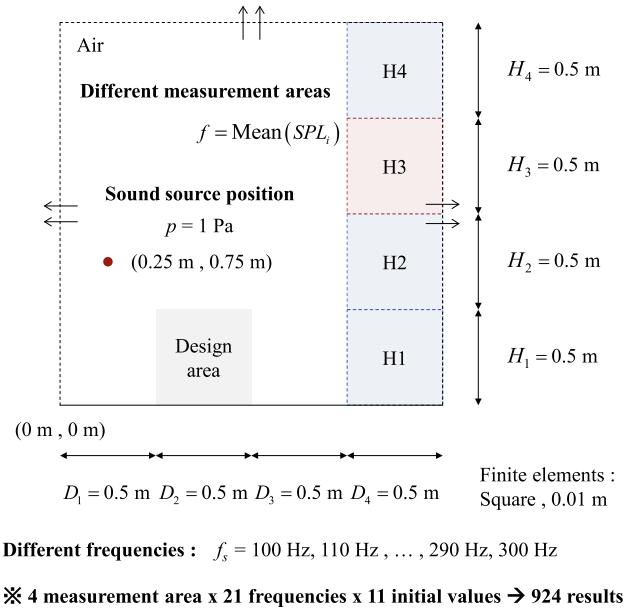

Fig. 11 Acoustic analysis conditions for the ground structure to be designed

structure built on the ground is treated as the design area, where topology optimization is performed. The FEA domain includes only the air area and design area, but not the area corresponding to the vertical structure. As depicted in Fig. 9, the solid line boundaries on the lower side of the acoustic domain represent the ground and perimeter of the vertical structure. At these boundaries, sound waves are reflected without transmission. On the contrary, dotted line boundaries represent the open border in the air, where sound waves propagate outward without reflection. In this example, a monopole sound source at a single frequency is situated on the left side of the design area, and a sound measurement area is specified on the right side of the design area.

The other design example for the duct internal structures is configured as shown in Fig. 10. In this example, a design area is positioned inside a straight duct, slightly separated from the inner wall of the duct. The upper and lower boundaries of the acoustic domain represent the inner walls of the duct with no sound transmission. At the left boundary, both incident and outgoing sound waves exist, and at the right boundary, only outgoing sound waves exist. In this example, a sound measurement area is specified near the outlet of the duct.

The third design example for ground structures is configured as shown in Fig. 11. This example has been modified in the barrier example. The design area is placed right above the ground. In this example, a monopole sound source is located higher than the height of the design area, and a sound measurement area is specified on the right side of the design area.

In the barrier example, the basic setting for the objective function to be minimized is set to the mean value of $|p|^2$ in the measurement area. In contrast, in the duct example and ground structure example, the basic setting for the objective function is set to the mean value of the SPL in the measurement area. The number of MMCs to form the structure in the design area is also different in each design example. The design examples for the barrier structure, the duct internal structure, and the ground structure use 4, 10, and 9 MMCs, respectively. The geometric parameters of the MMCs are determined by design variables according to the settings in Table 4. The basic settings for the initial values of design

Table 4 Geometric settings of MMCs for the design examples

Design example	n_c	$L_{\min}$	$L_{\max}$	$t_{\min}$	$t_{\max}$	$\theta_{\max}$	D_{design}	H_{design}
Barrier structure	4	0.1 m	0.5 m	0.04 m	0.04 m	2π	0.5 m	0.5 m
Duct structure	10	0.1 m	0.5 m	0.03 m	0.05 m	2π	0.5 m	0.5 m
Ground structure	9	0.1 m	0.5 m	0.04 m	0.04 m	2π	0.5 m	0.5 m

Table 5 Basic settings for the initial values of design variables in MMC-based topology optimization

Design example	Initial values of design variables
Barrier structure	$x_1 \sim x_{n_c} = 0$, $x_{n_c+1} \sim x_{2\times n_c} = 1/8$
	$x_{2\times n_c+1} = 0.1, x_{2\times n_c+2} = 0.5, x_{2\times n_c+3} = 0.5, x_{2\times n_c+4} = 0.9$
	$x_{3\times n_c+1} = 0.5, x_{3\times n_c+2} = 0.1, x_{3\times n_c+3} = 0.9$, $x_{3\times n_c+4} = 0.5$
Duct structure	$x_1 \sim x_{2\times n_c} = 0$
	$x_{2\times n_c+1} \sim x_{3\times n_c} = 1/8$
	$[x_{3\times n_c+1} \sim x_{4\times n_c}] = 0.1, 0.5, 0.9, 0.2, 0.4, 0.6, 0.8, 0.1, 0.5, 0.9$
	$x_{4\times n_c+1} \sim x_{4\times n_c+3} = 0.1, x_{4\times n_c+4} \sim x_{4\times n_c+7} = 0.5, x_{4\times n_c+8} \sim x_{4\times n_c+10} = 0.9$
	(random cases) $x_1 \sim x_{2\times n_c} = 0, x_{2\times n_c+1} \sim x_{5\times n_c} = x_{random} (0 \le x_{random} \le 1)$
Ground structure	$x_1 \sim x_{n_c} = 0, x_{n_c+1} \sim x_{2\times n_c} = 1/8$
	$x_{2\times n_c+1} \sim x_{2\times n_c+3} = 0.1, x_{2\times n_c+4} \sim x_{2\times n_c+6} = 0.5, x_{2\times n_c+7} \sim x_{2\times n_c+9} = 0.9$
	$x_{3\times n_c+1}, x_{3\times n_c+4}, x_{3\times n_c+7} = 0.1, x_{3\times n_c+2}, x_{3\times n_c+5}, x_{3\times n_c+8} = 0.5, x_{3\times n_c+3}, x_{3\times n_c+6}, x_{3\times n_c+9} = 0.9$
	(random cases) $x_1 \sim x_{n_c} = 0, x_{n_c+1} \sim x_{4\times n_c} = x_{random} (0 \le x_{random} \le 1)$

variables in MMC-based topology optimization are listed in Table 5.

4.2 MMC-based topology optimization results for target design conditions

In the design example for barrier structures, a case study was conducted to see the effect of the objective function, the initial layout of MMCs, and the number of MMCs on the MMC-based topology optimization results. Among the design conditions depicted in Fig. 9, the sound source position (1 m, 0 m), the measurement area "Mid 3", and the three frequencies (100 Hz, 200 Hz, and 300 Hz) are used as target design conditions for optimization. Figure 12 presents the layout of the MMCs as the iteration number of the optimization process increases under the frequency of 100 Hz. Each image depicts the values of the material interpolation parameters in the design area. Starting from the initial layout, separated MMCs join to form a shape.

Figure 13 shows the optimization results for the target design conditions using the two different objective functions in Eq. (28). In Fig. 13, the optimization results are displayed as an optimized shape that has been postprocessed. In each of the cases with three different frequencies, the optimized shape when the objective function is set to the mean of $|p|^2$ does not appear considerably different from the optimized shape when the objective function is set to the mean of the SPL. The target performance based on the optimized shape is also similar for the two objective functions. The target performance herein refers to the mean SPL for the design conditions under which the optimization was conducted. However, similar results cannot be generalized for the two objective functions.

MMC-based topology optimization can start with various initial layouts of MMCs. Figure 14 depicts the optimization results for four different initial layouts. From the optimization results shown in Fig. 14a, the effect of the initial layout on the optimized shape does not seem to be significant. However, in the optimization results of Fig. 14b which were obtained for the measurement area "Mid 2" instead of the measurement area "Mid 3", different initial layouts generate quite different optimized shapes.

The number of MMCs is also an important consideration for deriving an appropriate shape. Figure 15 depicts the optimization results for 9 MMCs and 16 MMCs. In the case of 100 Hz, the effect of increasing the number of MMCs is confirmed by the optimized shape change and the performance improvement compared with the results in Fig. 14a. In the case of 200 Hz and 300 Hz, the increased number of MMCs causes more complex shapes with slight performance improvement. In the design example for the barrier structure, four MMCs are used considering the design of a relatively simple shape.

In the design example for duct internal structures, the three frequencies (100 Hz, 200 Hz, and 300 Hz) are used as the target design conditions for optimization. Similarly, in the design example for ground structures, the measurement area "H3" and the three frequencies (100 Hz, 200 Hz, and 300 Hz) are used as the target design conditions for optimization. For these two design examples, Figs. 16 and 17 show the postprocessed optimization results for the target design conditions when the initial values of design variables are set

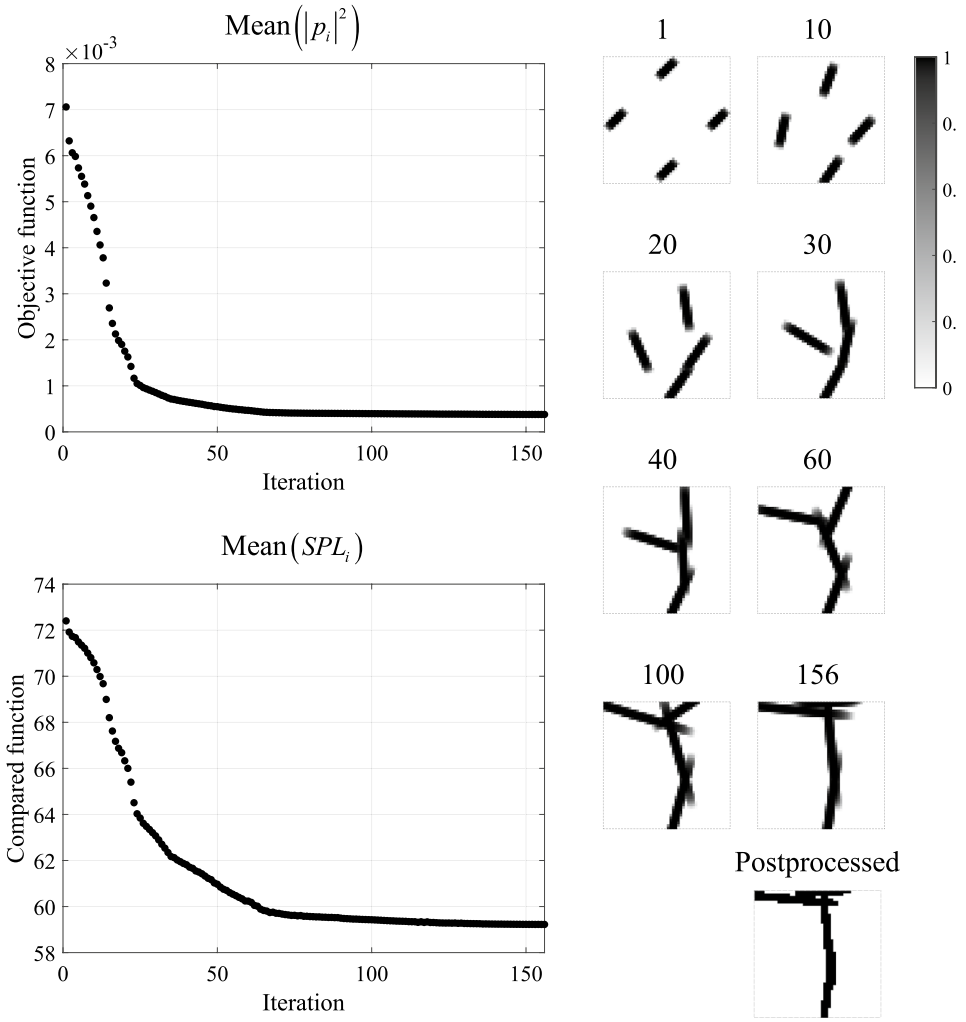

Fig. 12 Change of objective function value during optimization and layouts of MMCs in some iteration numbers

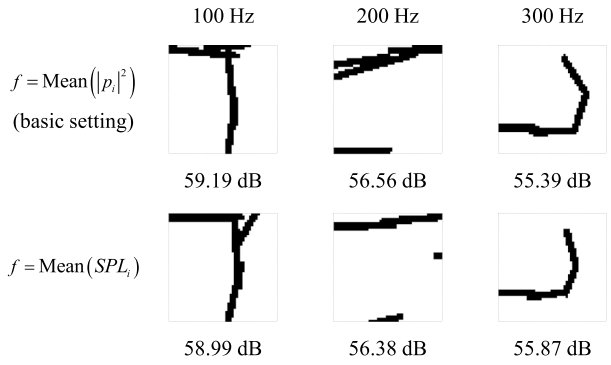

※ Value (dB) below the image indicates the target performance.

Fig. 13 Optimization results for the target design conditions (source position (1 m, 0 m) and measurement area "Mid 3") in the barrier example using different objective functions

to the basic setting and the random case "random 1". From these results, it can be seen that irregular initial layouts of MMCs by randomized design variables can provide different optimized layouts with improved target performance.

4.3 Comparison with SIMP-based topology optimization results

In this subsection, the SIMP-based topology optimization results obtained with the same target design conditions as the MMC-based topology optimization are presented. In the presented SIMP-based topology optimization, the material interpolation parameters are expressed by the design variables using a linear filter in Eq. (45). The weight value $w_{j,i}$ is calculated by the filter radius R and the distance $d_{j,i}$ between the j-th and i-th finite elements. The filter radius R is set to 0.025 m. The constraint parameter b, representing the

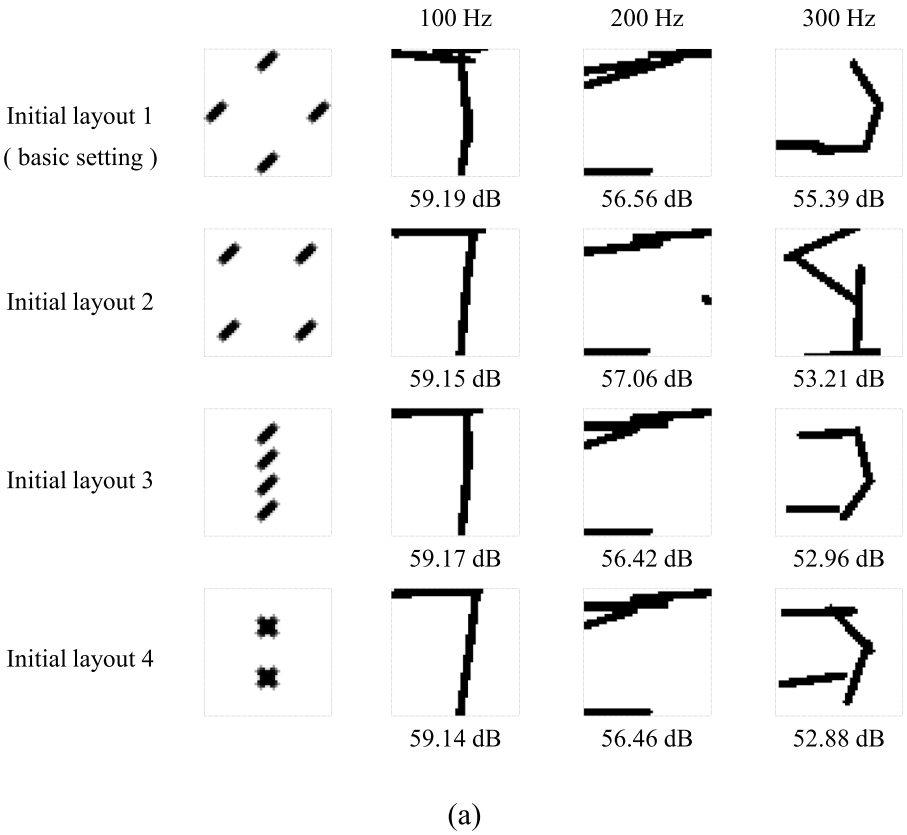

Fig. 14 Optimization results for different initial layouts of MMCs under the design conditions of **a** the measurement area "Mid 3" and **b** the measurement area "Mid 2" (barrier example)

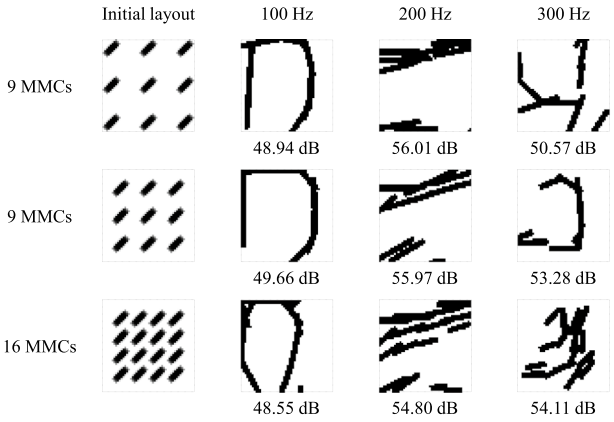

Fig. 15 Optimization results for different numbers of MMCs (barrier example)

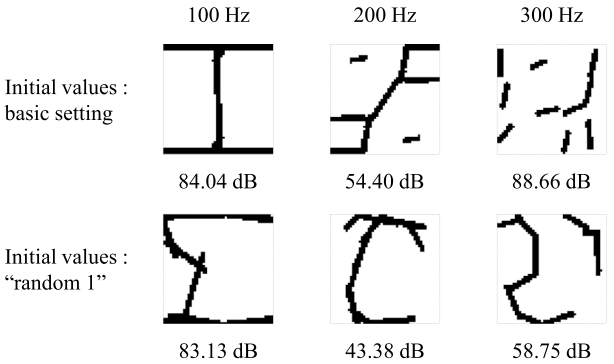

Fig. 16 Optimization results for the target design conditions in the duct example

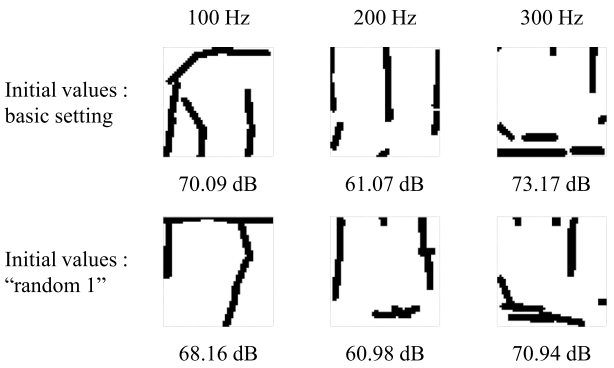

Fig. 17 Optimization results for the target design conditions (measurement area "H3") in the ground structure example

maximum occupancy rate of the rigid materials, is set to 0.3. The initial value of the design variables is set to 0.3, which is the same as the constraint parameter b. The initial value of the move range is set to 0.2, considering the appropriate change of material distribution. The objective function used for the SIMP-based topology optimization is the same as the basic setting used for the corresponding MMC-based topology optimization.

$$\gamma_j = \frac{\sum_{i=1}^{n_d} w_{j,i} x_i}{\sum_{i=1}^{n_d} w_{j,i}}, w_{j,i} = \max(0\,,\, R - d_{j,i}) \tag{45}$$

Figure 18a presents the SIMP-based optimization results in the barrier example, which is compared to the MMC-based optimization results in Fig. 13. The postprocessed SIMP-based shapes are not exactly the same as the corresponding MMC-based shapes. However, compared with the shapes in Fig. 15 using 9 MMCs, similar visual characteristics can be identified in the optimized shapes at 100 Hz and 200 Hz frequencies. Figure 18b shows the SIMP-based topology optimization results in the duct example, which is compared to the MMC-based optimization results in Fig. 16. Unlike the MMC-based shapes, the SIMP-based shapes show symmetrical shapes vertically and horizontally. Figure 18c shows the SIMP-based topology optimization results in the ground structure example, which is compared to the MMC-based optimization results in Fig. 17. Although there are some differences in the optimized shapes according to the two methods, it can be seen that some MMCs are arranged where rigid materials are mainly distributed in the SIMP-based method. Depending on the design example, the similarity between the MMC-based optimized shape and the SIMP-based optimized shape can differ.

SIMP-based acoustic topology optimization is difficult to derive complex shapes because it uses filter techniques to prevent irregular patterns of gray elements. This can be seen as one reason for the phenomenon that SIMP-based optimization results are somewhat different from MMC-based optimization results, even if the design conditions are the same. Another reason is that the MMC-based acoustic topology optimization is generally sensitive to the initial values of design variables and provides various local optimal solutions. The sensitivity of MMC-based optimized designs to the initial design variables can be confirmed in the following subsections. In this study, since SIMP-based designs are not investigated in detail under various conditions, it cannot be determined which optimization method is better in terms of target performance improvement. Nevertheless, the MMC-based design method has advantages over the SIMP-based design method in that various irregular shapes can be derived and there is a possibility of additional performance improvement.

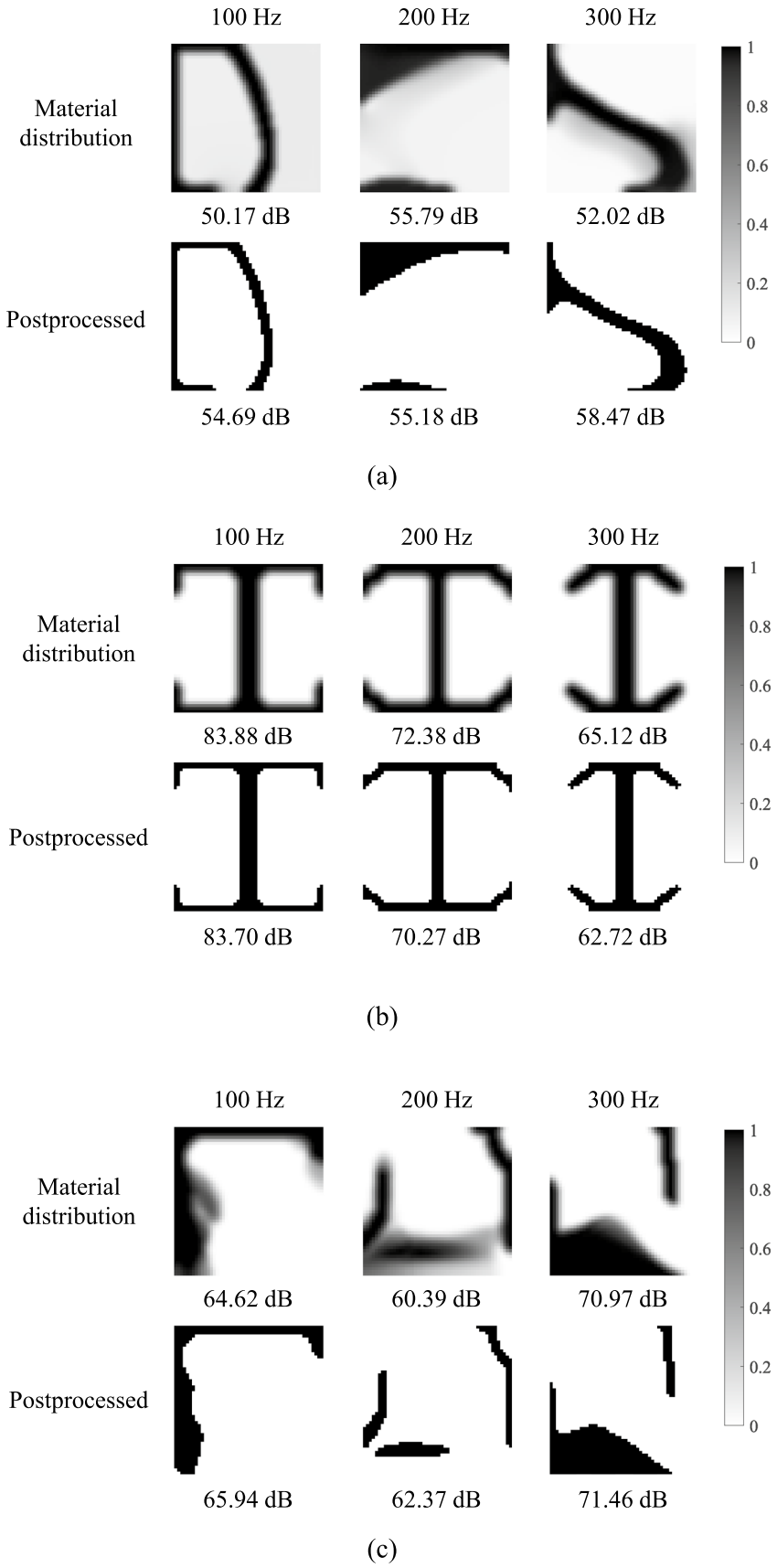

Fig. 18 Optimization results using the SIMP-based topology optimization in **a** the barrier example, **b** the duct example, and **c** the ground structure example

4.4 Additional design exploration using MMC-based topology optimization results

According to the design procedures presented in Sect. 3, a better design with an improved target performance is explored from MMC-based topology optimization results. The target performance refers to the mean SPL in the measurement area. In the design example for barrier structures, the target performance is calculated for the sound source position (1 m, 0 m) and the measurement area "Mid 3". In the design example for ground structures, the target performance is calculated for the measurement area "H3". Design explorations are carried out independently for the target performances at three frequencies: 100, 200, and 300 Hz.

4.4.1 Basic design samples

To generate multiple design samples, topology optimization was performed on the combinations of different design conditions and optimization conditions. In the barrier example, 9 sound source positions, 12 measurement areas, and 21 frequencies were considered, as depicted in Fig. 9. The frequencies were set at 10 Hz intervals. In the duct example, 2 types of objective functions, 26 frequencies, and 20 initial values of design variables were considered, as depicted in Fig. 10. The initial design variables were set to 20 random cases as described in Table 5. In the ground structure example, 4 measurement areas, 21 frequencies, and 11 initial values of design variables were considered, as depicted in Fig. 11. The initial design variables were set to one basic setting and 10 random cases, as described in Table 5. Therefore, the number of basic design samples is 2268, 1040, and 924 in each design example. Figure 19 depicts some basic design samples in the three examples.

4.4.2 Extracted design samples and modified design samples

In the barrier example, the top 200 design samples, according to the target performance, were extracted from the basic design samples. Table 6 presents the target performances of the highest, 200th, and lowest ranking for the basic design samples. Considering the performance of the 200th ranking, it can be observed that the top 200 design samples have relatively superior performance. Figure 20 illustrates the 200 extracted design samples based on the performance at the frequency of 100 Hz. The numbers of extracted design samples in the duct example and the ground structure are 100 and 50, respectively. 110,000 modified design samples were generated from the extracted design samples. Figure 21 depicts several design samples modified from one of the extracted design samples in the barrier example.

4.4.3 Candidate design samples and final design samples

10,000 candidate design samples were selected from the modified design samples based on the target performance estimated by the MLP. In the MLP estimation model, the size of the input vector is 2500, which is the number of finite elements in the design area. Table 7 presents the settings for the basic hyperparameters of the MLP used in the three design examples. The batch size and the standard deviation of the initial weights were slightly changed according to the design examples for appropriate training of the MLP. To test the estimation accuracy of the trained MLP, the estimated performances of the test design samples were compared with the accurate performances by FEA. Figure 22 presents the estimation results for the 300 samples among 2,000 test design samples in the barrier example. The comparison of the performance at 100 Hz indicates that the estimates are remarkably consistent with accurate performances. However, the estimation accuracies for the performances at 200 and 300 Hz are relatively lower than that for the performance at 100 Hz. The top 10 final design samples based on the accurate target performance by FEA were selected from the candidate design samples as Fig. 23.

4.5 Discussion on design results

In this subsection, the best performance of the basic design samples, the best performance of the modified design samples used to train the MLP, and the best performance of the final design samples are compared. Figures 24, 25, and 26 represent the compared design samples and their target performances in the three design examples, respectively.

First, the best performance of the basic design samples is generally much better than the performance of the design obtained by the local optimal point for the target design condition. Because of the local optima issue, it is interestingly observed in the case of the acoustic topology optimization that one local optimum for a different condition, i.e., the frequency, the target area for sound reduction, and the position of sound source, shows the superior performance for the target condition. This means that various topological designs based on the local optimal points should be obtained under various design conditions that are different from the original design condition. In addition, in the cases of the duct example and the ground structure example, it can be seen that various initial design variables help to find better designs.

In the three examples, the best performance of the modified design samples for training represents additional performance improvement compared with the best performance of the basic design samples. From the numerical tests in the present study, the best design of the modified design samples

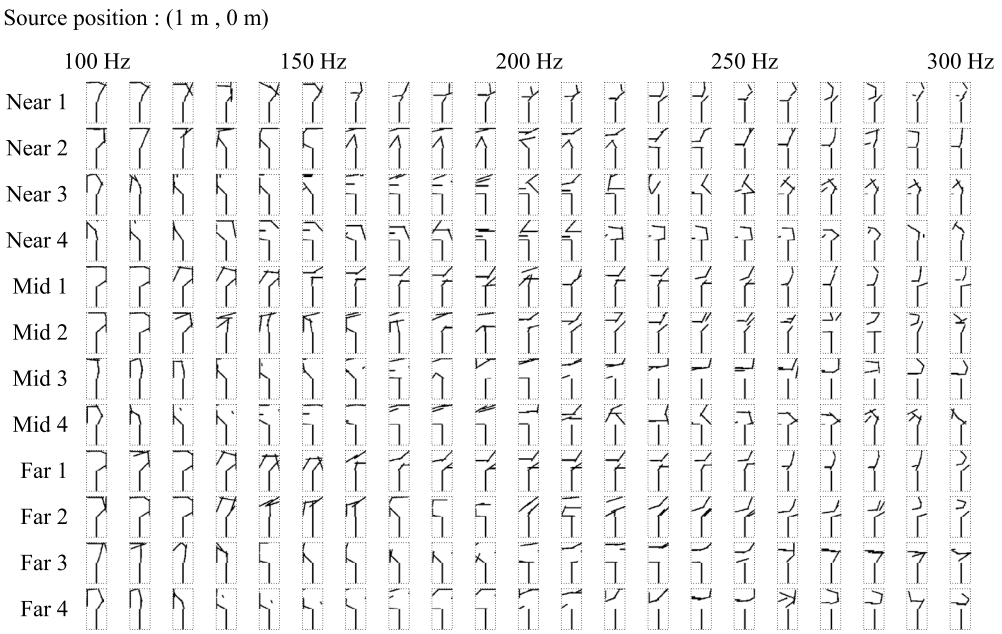
Source position : (1 m , 0 m)
100 Hz
150 Hz
200 Hz
250 Hz
300 Hz
Near 1
Near 2
Near 3
Near 4
Mid 1
Mid 2
Mid 3
Mid 4
Far 1
Far 2
Far 3
Far 4

(a)

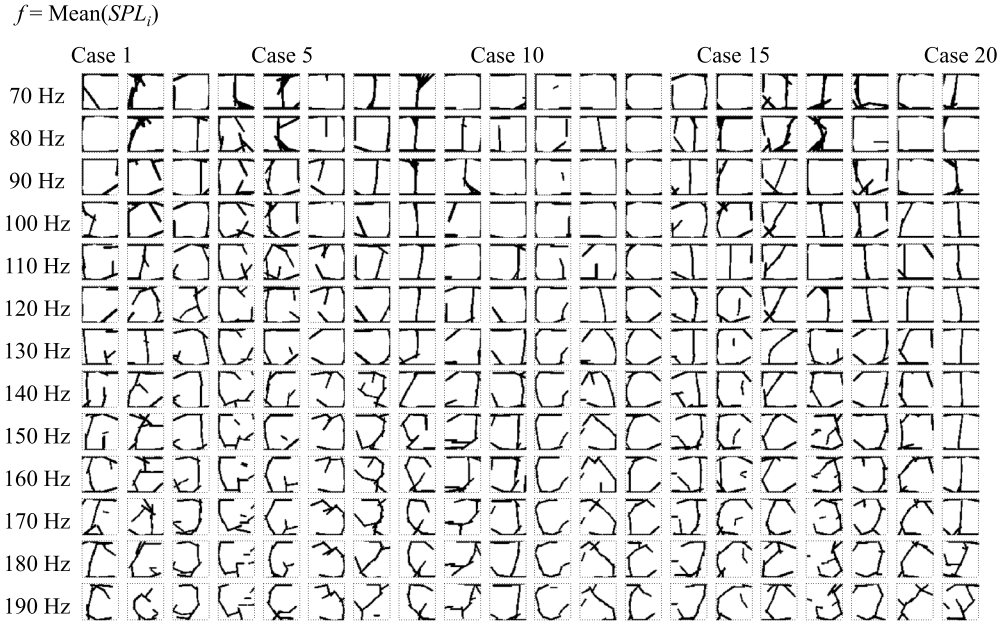
f = Mean(SPL_i)
Case 1
Case 5
Case 10
Case 15
Case 20
70 Hz
80 Hz
90 Hz
100 Hz
110 Hz
120 Hz
130 Hz
140 Hz
150 Hz
160 Hz
170 Hz
180 Hz
190 Hz

(b)

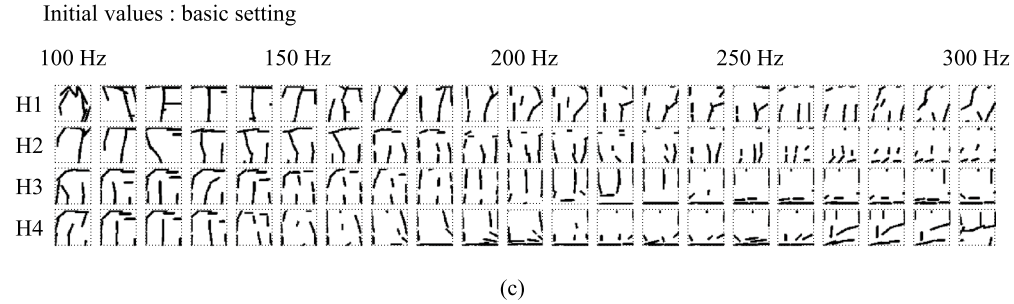
Initial values : basic setting
100 Hz
150 Hz
200 Hz
250 Hz
300 Hz
H1
H2
H3
H4

(c)

◂**Fig. 19** Basic design samples obtained from MMC-based topology optimization results in **a** the barrier example, **b** the duct example, and **c** the ground structure example

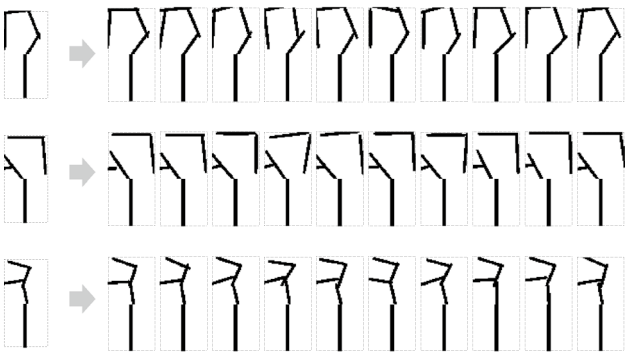

Fig. 21 Examples for modification of a design sample (barrier example)

was not obtained from the best design of the basic design samples. The value in the parenthesis below the target performance indicates the index of the corresponding extracted design sample. In other words, the designs with the same values in parentheses were modified from the same design sample. This fact also supports the importance of obtaining various design samples. Due to the acoustic characteristics of sound waves, there was a change in target performance even though the geometric values for MMCs were slightly modified.

The best performance of the final design samples can also represents additional performance improvement compared with the best performance of the modified design samples for training. However, the degree of performance improvement is different in each design example. In the barrier example, the degree of performance improvement is less than 1 dB in the case of 100 Hz. In the case of 200 Hz, the best performance of the final design samples is not better than that of the modified design samples for training. In the duct example, the best performance of the final design samples is better than that of the modified design samples for training in all cases of three frequencies. However, in the case of 300 Hz, the degree of performance improvement is less than 1 dB. In the ground structure example, when 10,000 candidate design samples were analyzed, the best performance of the final design samples is better than that of the modified design samples for training only in the case of 300 Hz. Accordingly, the number of candidate design samples analyzed was increased to 20,000, which corresponds to the top 20% based on the estimated performance. As a result, performance improvement could be achieved

Table 6 Target performances of the design samples in the highest, 200th, and lowest ranking among the basic design samples

Barrier example	Mean SPL at 100 Hz	Mean SPL at 200 Hz	Mean SPL at 300 Hz
Sample of the highest ranking	49.95 dB	52.90 dB	38.25 dB
Sample of the 200th ranking	59.42 dB	59.55 dB	56.32 dB
Sample of the lowest ranking	74.38 dB	72.89 dB	70.58 dB

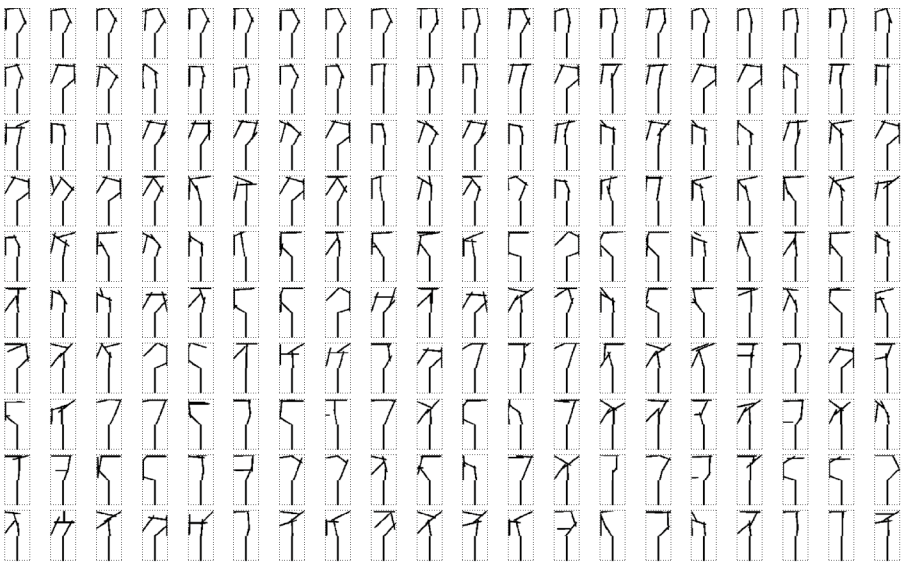

Fig. 20 200 extracted design samples based on the target performance at 100 Hz frequency (barrier example)

Table 7 Settings for the hyperparameters of MLP

Design example	Batch size	Number of hidden layers	Hidden layer sizes	Learning rate	Number of epochs	Mean and standard deviation of initial weights
Barrier structure	10	4	64, 32, 16, 8	0.001	50	0, 0.001
Duct structure	20	4	64, 32, 16, 8	0.001	50	0, 0.005
Ground structure	10	4	64, 32, 16, 8	0.001	50	0, 0.005

in all cases of three frequencies. However, in the case of 200 Hz, the performance improvement is still less than 1 dB. The best performance of the final design samples obtained when only 1,000 candidate design samples were analyzed is also presented. However, in this case, the performance did not improve or the performance improvement is almost less than 1 dB. Therefore, the selection of 1,000 candidate design samples is insufficient. The three design examples show that the additional design procedures presented in this study may help improve the performance of MMC-based acoustic structures.

Figure 27 depicts the SPL distributions for the best designs of the basic design samples, the modified design samples for training, and the final design samples. It can be seen that the average SPL in the target performance measurement area decreases through the additional design process.

5 Conclusions

In this study, we investigated the possibility of applying MMC-based topology optimization to the acoustic design problem. Despite the advantages of the topology optimization method that generates novel shapes of structures, topological designs by certain local optimal points did not guarantee sufficiently satisfactory performance in the presented design examples. Therefore, we evaluated various designs optimized for different design conditions and optimization settings. Because the local optimum design under a nontargeted design condition is not a local optimum design under the targeted design condition, performance improvement for the targeted design condition was achieved through slight shape modification. In the additional design procedures through shape modification, we investigated the feasibility of MLP as a performance estimation model.

Although an appropriate selection of candidate design samples through the performance estimation by the MLP was possible in the present study, there are many challenges related to the estimation accuracy. As the degree of shape modification increases, it is advantageous to explore various

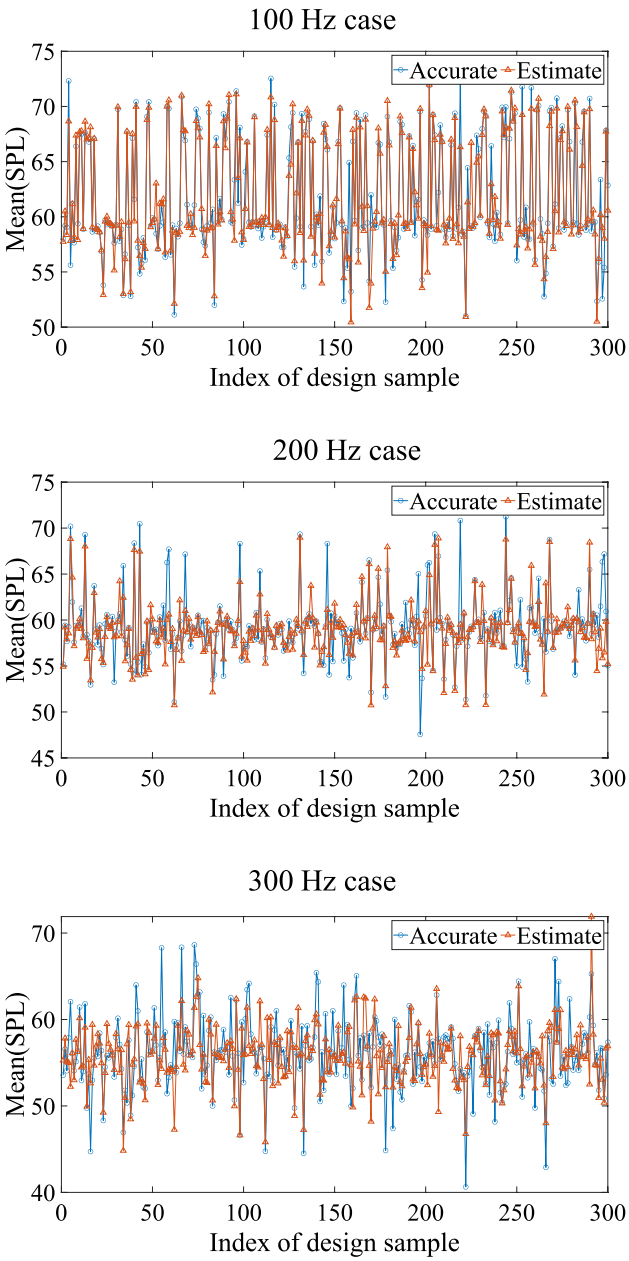

Fig. 22 Estimated performances of MLP for the test design samples (barrier example)

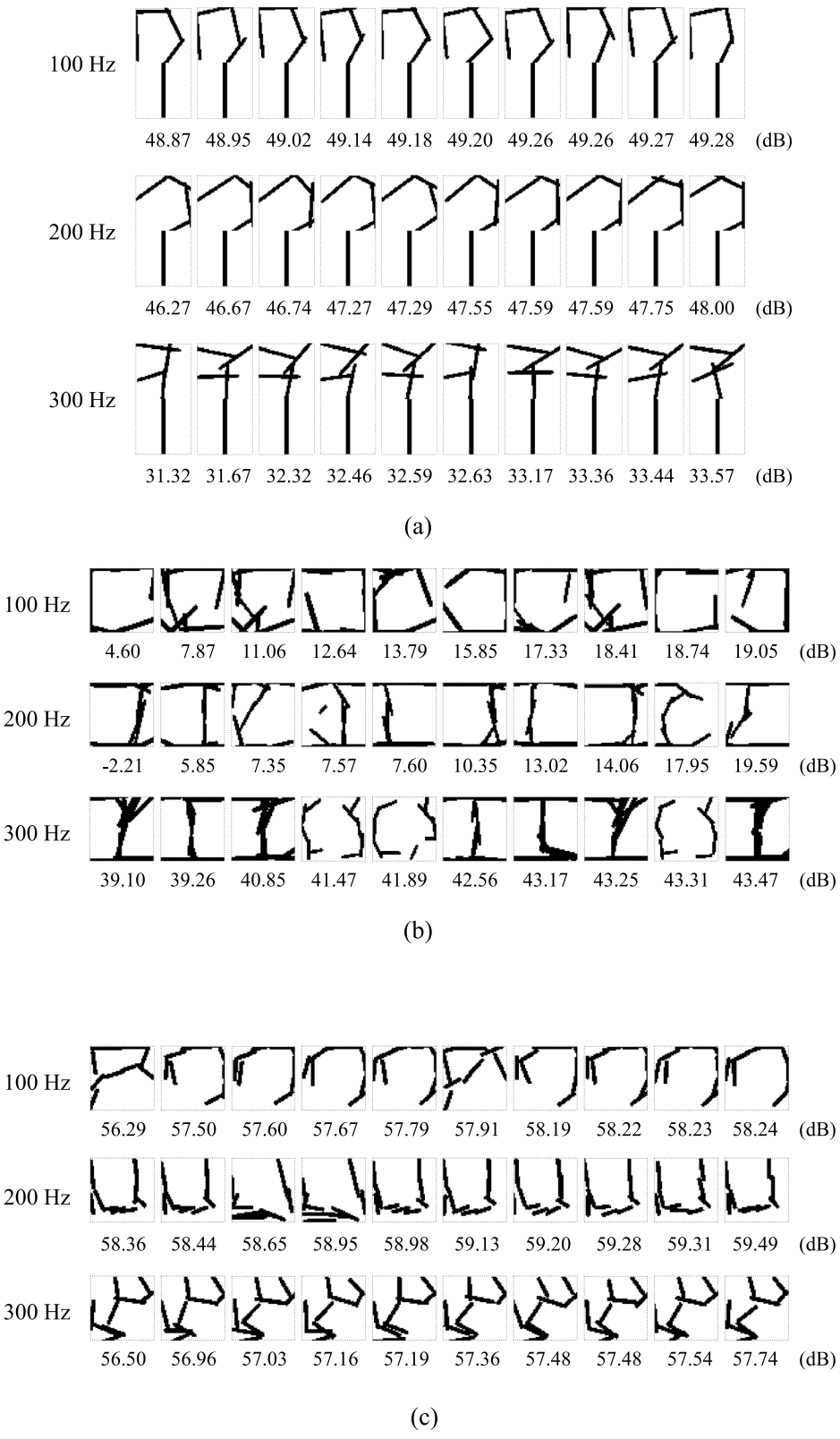

Fig. 23 Top 10 final design samples selected from candidate design samples in **a** the barrier example, **b** the duct example, and **c** the ground structure example

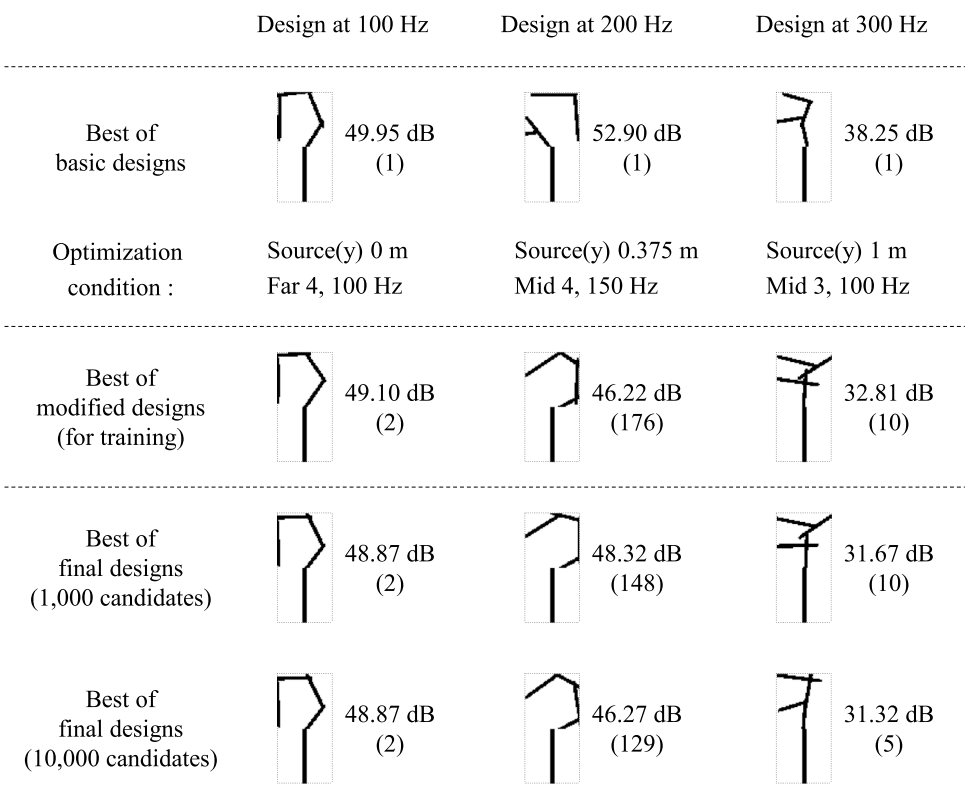

※ Value in parenthesis : index of the corresponding extracted design sample

Fig. 24 Comparison of best performances of different groups of design samples (barrier example)

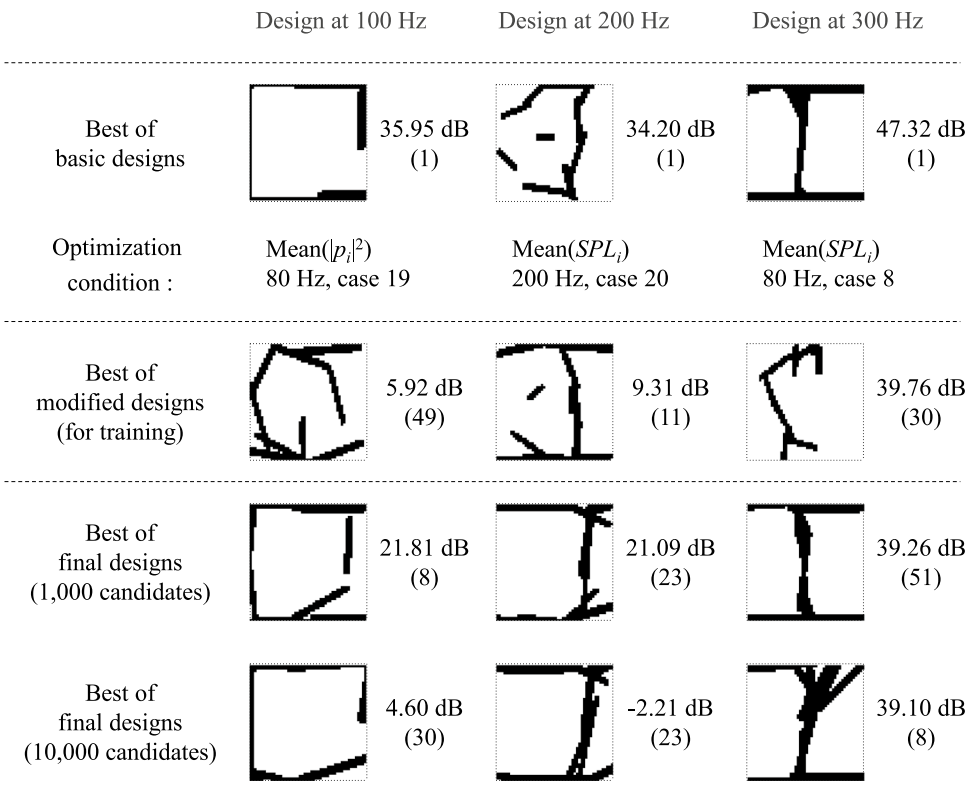

※ Value in parenthesis : index of the corresponding extracted design sample

Fig. 25 Comparison of best performances of different groups of design samples (duct example)

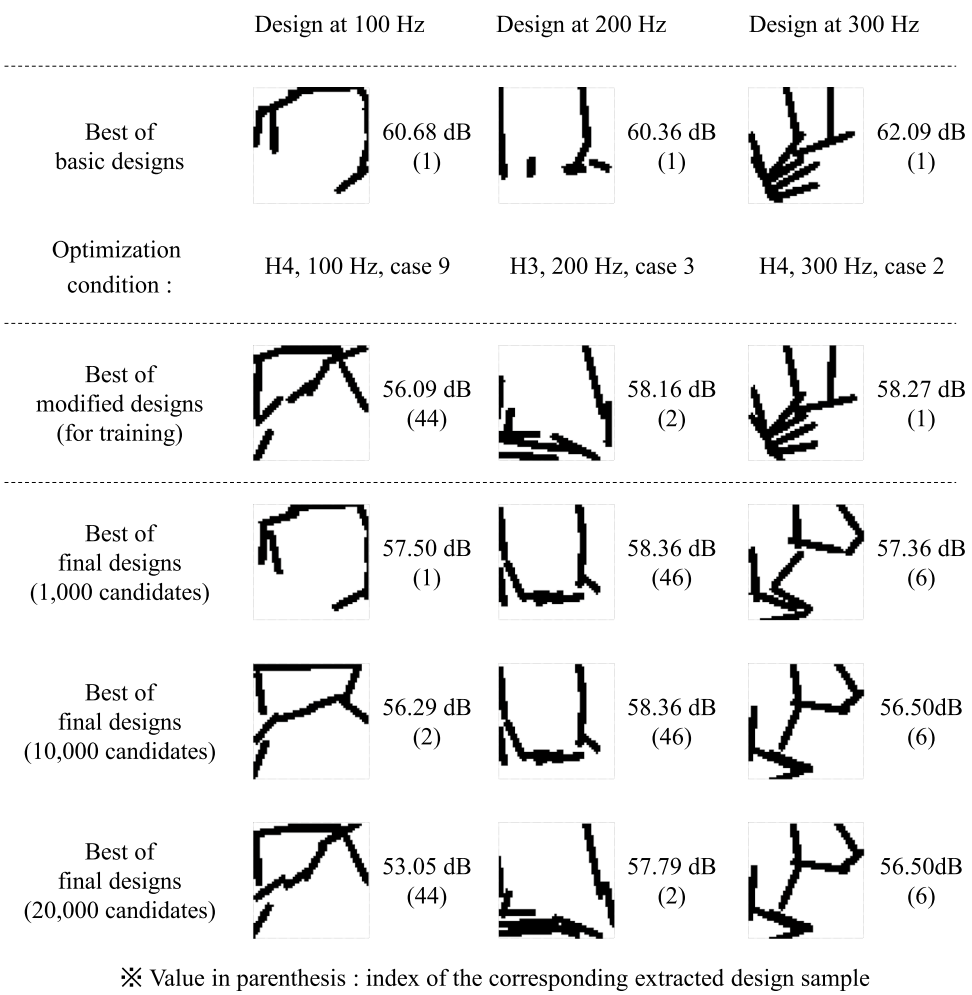

※ Value in parenthesis : index of the corresponding extracted design sample

Fig. 26 Comparison of best performances of different groups of design samples (ground structure example)

design samples with different characteristics in the overall shape, but it becomes more difficult to estimate the performance with high accuracy using an MLP. In other words, as the relationship between structural design information and acoustic performance exhibits high nonlinearity (complexity), training the neural network becomes more difficult. Therefore, the number of extracted design samples subjected to shape modification and the degree of shape modification should be appropriately considered.

In the future, a study to improve the estimation accuracy of ANNs will be conducted. For example, a CNN specialized for image recognition could be used instead of an MLP. Furthermore, optimization methods other than the gradient descent method could be used to train an ANN. Changing the regression problem in this study to a multiclass classification problem could also be an alternative. In this case, it would be possible to define several categories corresponding to the ranges that distinguish the performance values. Then, design samples could be classified according to the category predicted by an ANN.

To conclude, this study proposes a systematic design approach for a sound reduction structure based on MMC-based topology optimization. The main idea of the proposed design approach is simple, but it is meaningful in that it complements the limited design results obtained using only topology optimization. Our approach helps not only to find a single design with the best performance, but also to explore various designs with different shapes and similar

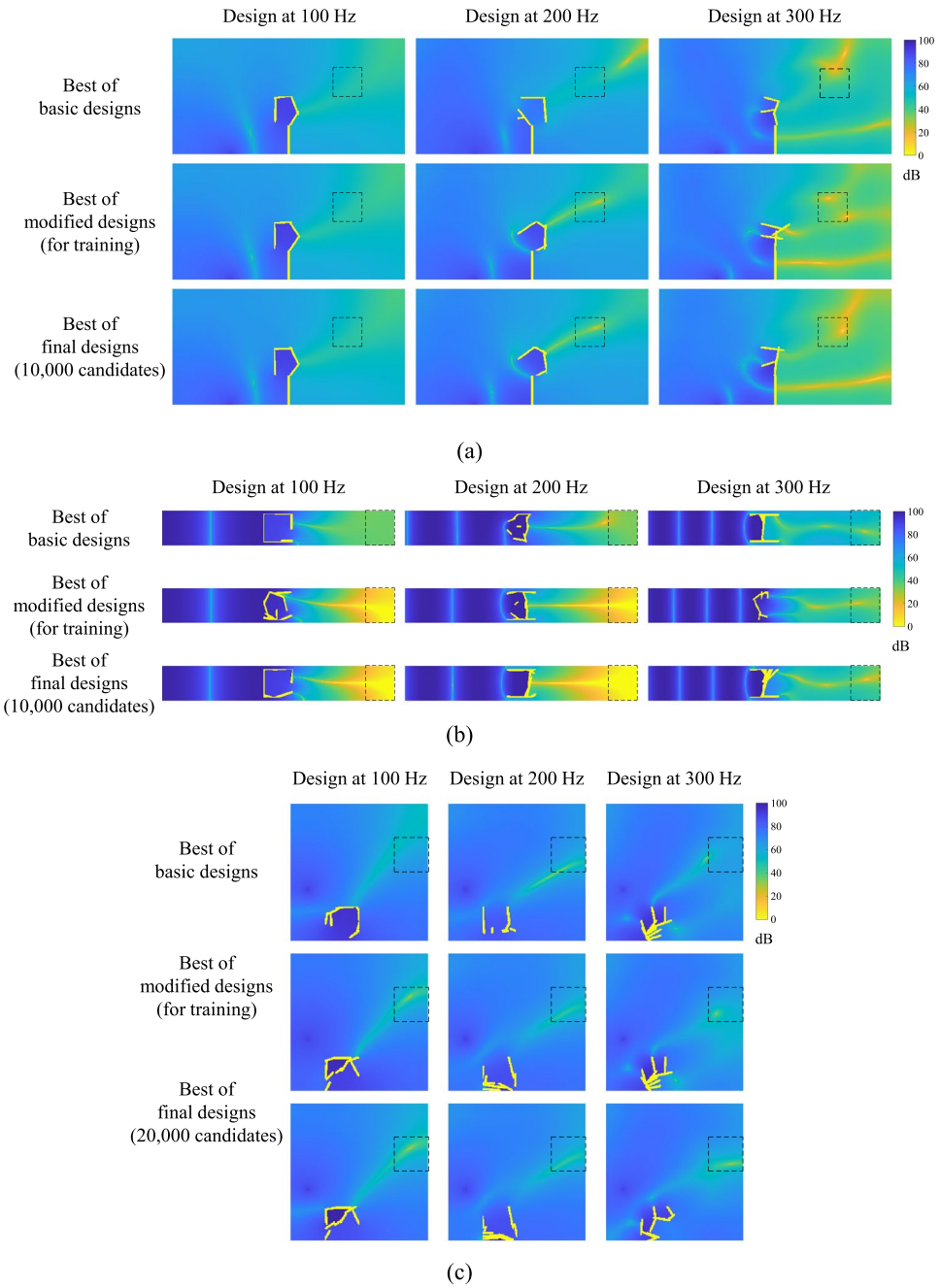

Fig. 27 Distributions of SPL for best designs of different groups of design samples in **a** the barrier example, **b** the duct example, and **c** the ground structure example

performances. Of course, there may be more effective and practical design strategies than the design method proposed in this study, but the design examples presented in this study may be beneficial in inspiring researchers to create new and varied design methods.

Authors' contributions Conceptualization and methodology: Ki Hyun Kim and Gil Ho Yoon; Investigation and writing: Ki Hyun Kim; Review: Gil Ho Yoon; Funding acquisition and supervision: Gil Ho Yoon.

Funding This work was supported by the National Research Foundation of Korea (NRF) grant funded by the Korea government (MSIT) (NRF-2019R1A2C2084974).

Data availability Not applicable.

Code availability Not applicable.

Declarations

Conflict of interest The authors declare that they have no conflict of interest.

Ethical approval Not applicable.

Replication of results The presented results were mainly obtained using our in-house MATLAB codes and may be provided on reasonable request.

Consent to participate Not applicable.

Consent for publication Not applicable.

References

Chang YC, Chiu MC, Wu MR (2018) Acoustical assessment of automotive mufflers using FEM, neural networks, and a genetic algorithm. Arch Acoust 43(3):517–529

Christiansen RE, Lazarov BS, Jensen JS, Sigmund O (2015) Creating geometrically robust designs for highly sensitive problems using topology optimization. Struct Multidisc Optim 52(4):737–754

Deng JD, Chen W (2016) Design for structural flexibility using connected morphable components based topology optimization. Sci China Technol Sc 59(6):839–851

Duhring MB, Jensen JS, Sigmund O (2008) Acoustic design by topology optimization. J Sound Vib 317(3–5):557–575

Durali M, Delnavaz A (2005) BEM/FEM simulation of acoustic field and shape optimization of submarine using neural network and genetic algorithm. Proceedings of the 2004 International Symposium on Underwater Technology (IEEE Cat. No.04EX869)

Goo S, Wang S, Kook J, Koo K, Hyun J (2017) Topology optimization of bounded acoustic problems using the hybrid finite element-wave based method. Comput Method Appl M 313:834–856

Guo X, Zhang WS, Zhong WL (2014) Doing topology optimization explicitly and geometrically-a new moving morphable components based framework. J Appl Mech-T Asme Doi 10(1115/1):4027609

Guo X, Zhang WS, Zhang J, Yuan J (2016b) Explicit structural topology optimization based on moving morphable components (MMC) with curved skeletons. Comput Method Appl M 310:711–748

Guo X, Li W, Iorio F (2016a) Convolutional neural networks for steady flow approximation. Proceedings of the 22nd ACM SIGKDD International Conference on Knowledge Discovery and Data Mining

Kim KH, Yoon GH (2020) Aeroacoustic topology optimization of noise barrier based on Lighthill's acoustic analogy. J Sound Vib 483

Kim KH, Yoon GH (2015) Optimal rigid and porous material distributions for noise barrier by acoustic topology optimization. J Sound Vib 339:123–142

Kook J, Koo K, Hyun J, Jensen JS, Wang S (2012) Acoustical topology optimization for Zwicker's loudness model - application to noise barriers. Comput Method Appl M 237:130–151

Kook J, Jensen JS, Wang S (2013) Acoustical topology optimization of Zwicker's loudness with Pade approximation. Comput Method Appl M 255:40–66

Lee JW (2015) Optimal topology of reactive muffler achieving target transmission loss values: design and experiment. Appl Acoust 88:104–113

Lee JW, Kim YY (2009) Topology optimization of muffler internal partitions for improving acoustical attenuation performance. Int J Numer Meth Eng 80(4):455–477

Lei X, Liu C, Du ZL, Zhang WS, Guo X (2019) Machine learning-driven real-time topology optimization under moving morphable component-based framework. J Appl Mech-T Asme https://doi.org/10.1115/1.4041319

Li BT, Huang CJ, Li X, Zheng S, Hong J (2019) Non-iterative structural topology optimization using deep learning. Comput Aided Design 115:172–180

Lian RC, Jing SK, He ZJ, Shi ZF, Song GH (2020) An accelerating convergence rate method for moving morphable components. Math Probl Eng 2020

Liang L, Liu ML, Martin C, Sun W (2018) A deep learning approach to estimate stress distribution: a fast and accurate surrogate of finite-element analysis. J R Soc Interface 15(138)

Nie ZG, Jiang HL, Kara LB (2020) Stress field prediction in cantilevered structures using convolutional neural networks. J Comput Inf Sci Eng 20(1)

Oh S, Jung Y, Kim S, Lee I, Kang N (2019) Deep generative design: Integration of topology optimization and generative models. J Mech Design 141(11)

Rai MM, Madavan NK (2001) Application of artificial neural networks to the design of turbomachinery airfoils. J Propul Power 17(1):176–183

Sosnovik I, Oseledets I (2019) Neural networks for topology optimization. Russ J Numer Anal M 34(4):215–223

Svanberg K (1987) The method of moving asymptotes - a new method for structural optimization. Int J Numer Meth Eng 24(2):359–373

Svanberg K (1998) The method of moving asymptotes - modelling aspects and solution schemes. Lecture notes for the DCAMM course

Svanberg K (2007) MMA and GCMMA - two methods for nolinear optimization. Technical report

Takalloozadeh M, Yoon GH (2017) Implementation of topological derivative in the moving morphable components approach. Finite Elem Anal Des 134:16–26

Ulu E, Zhang RS, Kara LB (2016) A data-driven investigation and estimation of optimal topologies under variable loading configurations. Comp M Bio Bio E-Iv 4(2):61–72

Yahya MN, Otsuru T, Tomiku R, Okozono T (2010) Investigation the capability of neural network in predicting reverberation time on classroom. International Journal of Sustainable Construction Engineering and Technology 1(1):19–32

Yilmaz E, German B (2017) A convolutional neural network approach to training predictors for airfoil performance. 18th AIAA/ISSMO Multidisciplinary Analysis and Optimization Conference

Yoon GH (2013) Acoustic topology optimization of fibrous material with Delany-Bazley empirical material formulation. J Sound Vib 332(5):1172–1187

Yoon GH, Choi H, Hur S (2018) Multiphysics topology optimization for piezoelectric acoustic focuser. Comput Method Appl M 332:600–623

Yu Y, Hur T, Jung J, Jang IG (2019) Deep learning for determining a near-optimal topological design without any iteration. Struct Multidisc Optim 59(3):787–799

Zhang WS, Yuan J, Zhang J, Guo X (2016) A new topology optimization approach based on moving morphable components (MMC) and the ersatz material model. Struct Multidisc Optim 53(6):1243–1260

Zhang WS, Li D, Zhou JH, Du ZL, Li BJ, Guo X (2018a) A moving morphable void (MMV)-based explicit approach for topology optimization considering stress constraints. Comput Method Appl M 334:381–413

Zhang Y, Sung W, Mavris D (2018b) Application of convolutional neural network to predict airfoil lift coefficient. 2018 AIAA/

ASCE/AHS/ASC Structures, Structural Dynamics, and Materials Conference

Zheng S, Fan HJ, Zhang ZY, Tian ZQ, Jia K (2021a) Accurate and real-time structural topology prediction driven by deep learning under moving morphable component-based framework. Appl Math Model 97:522–535

Zheng S, He ZZ, Liu HL (2021b) Generating three-dimensional structural topologies via a U-Net convolutional neural network. Thin Wall Struct 159:107263